Branched and Linear F-actin Networks Control Directional Migration Switching Behavior on Aligned Collagen Fibrils

Azarnoosh Foroozandehfar[1], *Shayan Tohidi*[2], *Shafayet Ahmed Siddiqui*[3], *Fred Rogers Namanda*[3] and *Ian C. Schneider*[1,4*‡]

[1]Department of Chemical and Biological Engineering, Iowa State University

[2]Department of Industrial and Manufacturing Systems Engineering

[3]Molecular, Cellular and Developmental Biology Program, Iowa State University

[4]Department of Genetics, Development and Cell Biology, Iowa State University

Present address: Iowa State University, Department of Chemical and Biological Engineering, 2114 Sweeney Hall, Ames, IA, 50011-2230, United State

‡Author for correspondence (phone: (515) 294-0450, fax: (515) 294-2689, e-mail: ians@iastate.edu)

Key Words:

mechanobiology, contact guidance, topotaxis, extracellular matrix, stiffness, epitaxial growth, mica

Abstract:

Directed cell migration is essential in biological processes like embryonic development, wound healing and cancer metastasis and is driven by a variety of directional cues, including aligned fibrils in the extracellular matrix (ECM), a phenomenon known as contact guidance. How different cells respond to aligned fibrils and how external factors like ECM stiffness and internal regulators like formins and Arp2/3 control contact guidance across different type of cells is unknown. In this study, a unique system to assemble aligned collagen fibrils on mica and to transfer them onto substrates with specified stiffness is used to probe how external factors and internal regulators affect contact guidance. This system reveals distinct contact guidance behaviors: mesenchymal cells exhibit high-fidelity contact guidance, amoeboid cells ignore cues and epithelial cells use a mixture of both parallel and perpendicular migration on aligned collagen fibrils. Formins and Arp2/3 exert reciprocal control over contact guidance across a variety of cell types, where formins mediators of linear F-actin structures enhance contact guidance and Arp2/3 a mediator of branched F-actin structures diminishes contact guidance. This controlled materials system reveals important external and internal mechanisms of how contact guidance directs cell migration across a variety of different cell types.

Graphical Abstract:

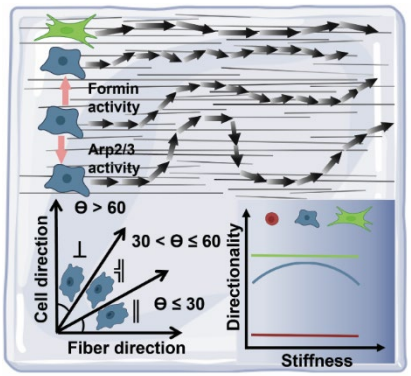

Abbreviations:

DPBS: Phosphate-Buffered Saline

BME (β-MercaptoEthanol)

APS: Ammonium Persulfate

APTES: 3-AminoPropylTriEthoxySilane

EGTA: Ethylene Glycol bis(2-aminoethyl ether)-N,N,N′,N′-Tetraacetic Acid

PVDF: Polyvinylidene DiFluoride

BSA: Bovine Serum Albumin

ECM: Extracellular Matrix

TEMED: N,N,N', N'-Tetraacetylethylenediamines

TBS: Tris Buffered Saline

HEPES: 2-hydroxyethylpiperazine-1-ethane sulfonic acid

FBS: Fetal Bovine Serum

DMSO: DiMethyl SulfOxide

MES: 2-N-Morpholino Ethane Sulfonic acid

ECL: Enhanced ChemiLuminescent

HFF: Human Foreskin Fibroblast

EMT: Epithelial to Mesenchymal Transition

AFM: Atomic Force Microscopy

p-myo: phosphorylated myosin

PAA: PolyAcrylAmide

af: Aligned Fibrils

tf: Transferred Fibrils

mdf: MultiDirectional Fibrils

rf: Random Fibrils

m: Mica

g: Glass

0.2: 200 Pa PAA gel

2: 2000 Pa PAA gel

20: 20,000 Pa PAA gel

1. Introduction:

Contact guidance refers to the directed migration of cells along aligned fibrils present in the extracellular matrix (ECM). Directional movement is crucial in a variety of biological processes. Studying contact guidance is particularly important because contact guidance controls embryonic development [1,2] and wound healing [3,4]. Contact guidance also impacts pathological conditions, directing migration in fibrosis and during cancer metastasis [5,6]. Contact guidance can be recreated *in vitro* using various methods, including electrospinning [7], which produces synthetic aligned fibrils; microcontact printing [8,9], which produces printed lines of ECM and grooves or ridges [10] that guide cellular movement topographically. While these are good at recapitulating certain geometric and chemical features, they lack ultrastructural signatures that are found on collagen fibrils assembled *in vivo*. Other approaches exist to make aligned collagen fibrils in 3D networks, including magnetic field alignment [11], mechanical rotation [12], flow-based alignment [13,14] or cell-based alignment [15–17]. Our lab has used a 2D self-assembly approach to make aligned collagen fibrils through epitaxial growth on mica, resulting in fibrils closely resembling those in tissues. We have developed methods to finely tune the structure of collagen fibrils on mica, allowing us to adsorb randomly oriented fibrils, bidirectional fibrils, aligned fibrils or no fibrils at all [18]. This approach allows for the observation of unique cellular responses to aligned collagen fibrils in comparison to other systems and has allowed for the characterization of the role of contractility and adhesion in tuning contact guidance, where mesenchymal cells contact guide well and amoeboid cells contact guide poorly [19]. These cell-type specific responses aren't visible with standard microprinting or topographical structures like ridges, but do replicate contact guidance behavior seen by mechanical alignment of collagen fibrils in 3D [12]. We also preliminarily explored a technique to transfer these fibrils onto glass, polydimethylsiloxane, and polyacrylamide gels [20], allowing us to initially probe how stiffness regulates contact guidance. Consequently, epitaxial growth of aligned collagen fibrils on mica affords a powerful approach to study contact guidance that retains ultrastructural characteristics of the collagen fibrils and mimics behavior seen in less tunable 3D contact guidance environments.

Cells within tissues have unique functions and, consequently, a unique set of genetic and signaling pathways that direct that behavior. The sensitivity of cells to contact guidance cues differs dramatically amongst cell types due to their differing roles within tissues. For instance, fibroblasts must remodel the ECM and generate contractile forces to provide mechanical stability of the wound. This frequently results in transient alignment of the ECM within the wound bed that enhances cell infiltration, including additional fibroblasts via contact guidance [3,21]. Over the long term, this alignment is destroyed once mechanical integrity and directed cell migration are no longer needed [22]. Epidermal keratinocytes on the other hand facilitate re-epithelialization outward in and may need to be less sensitive to fibril alignment, given that wounds frequently re-epithelialize uniformly from all directions [3]. Finally, immune

cells need to randomly surveil the wound microenvironment with no bias in migration in response to aligned collagen fibrils, requiring them to ignore contact guidance cues. Indeed, ECM fibril alignment seems not to enhance T cell infiltration into the tumor [23] and T cell contact guidance is low compared to other cell types [24]. Local cell invasion during cancer occurs along aligned collagen fibrils that extend radially from the tumor margin [25], but this primarily drives cancer cell and fibroblastic stromal contact guidance. This suggests that cells can be placed into groups based on their roles and these groups of cells have dramatically different abilities to sense and respond to contact guidance cues.

While early contact guidance work did not delineate between differences among cells of different type, more recent work indicates that there are dramatic differences in how cells sense and respond to contact guidance cues [26–29]. Different qualitative modes of migration have been described that have allowed for a coarse-grain understanding of cell migration. Mesenchymal cells adopt a spindle shape, showing strong adhesion and many stress fibrils, usually oriented parallel to the direction of migration. Epithelial cells adopt a half-moon shape with a broad lamellipodium, intermediate adhesive strength, and stress fibrils both parallel and perpendicular to the direction of migration. Amoeboid cells are rounded with low adhesion and few stress fibrils but with a cortical contractile and protrusive F-actin cytoskeleton. In addition, there are cells that can irreversibly or dynamically switch between epithelial and mesenchymal migration modes as well as those that switch between amoeboid and mesenchymal modes of migration [30,31]. Mesenchymal cells showed higher contact guidance than those undergoing epithelial-to-mesenchymal transition (EMT) [28,32]. Ameboid cells showed random alignment, while mesenchymal cells showed directed migration in both 2D and 3D systems [12,19]. However, these reports have mainly been on substrates that may obscure cell type differences *in vivo* [19]. A systematic examination of contact guidance across cell types in systems that present *in vivo* ECM structures is lacking. In particular, how epithelial cells respond to contact guidance cues is not well understood. In addition, there is a lack of understanding of how external signals like substrate stiffness and internal regulators of the F-actin cytoskeletal control the cell type difference in contact guidance behavior.

Contact guidance occurs in tissues with a variety of different stiffnesses according to the needs of the tissue. Stiffness can modulate a variety of different biophysical cellular aspects including traction force and adhesion, two factors that regulate contact guidance. Consequently, it is reasonable that stiffness affects contact guidance. Stiffness has been adjusted in various ways including increasing the stiffness of individual fibers, tuning the underlying substrate stiffness and enhancing crosslinking of 3D fiber networks [11,29,33–35]. On stiffer substrates, cells generate stronger traction forces, form more stable adhesions, and align more effectively with the ECM fibrils, enhancing their directional migration along these structures. In contrast, cells on soft substrates have weaker adhesions and traction forces, making their alignment with ECM fibrils and directional movement less pronounced. Furthermore, there is some

133 indication that the most efficient contact guidance tends to be at physiological stiffness levels of the
134 substrate. While there are many disparate studies on contact guidance and how stiffness regulates it, there
135 is no systematic study on how stiffness regulates contact guidance across multiple cells.

136 Differences in contact guidance across different cells could be attributed to differences in surface
137 receptors, but in instances where cells spread and migrate on a particular substrate, likely differences in
138 contact guidance are due to signaling pathways and cytoskeletal regulation. The F-actin cytoskeleton is an
139 important regulator of cell migration. Cells build both linear and branched F-actin networks that allow the
140 cell to migrate directionally. Formins and Arp2/3 regulate cell migration by controlling the organization
141 of the actin cytoskeleton. Formins, promote the formation of linear actin filaments, which are essential for
142 creating stress fibrils and contractile forces that drive cell body movement and stabilize cell adhesion.
143 Arp2/3 on the other hand is responsible for forming branched actin networks, which are crucial for
144 generating the pushing forces needed for forming lamellipodia and protrusions at the leading edge of
145 migrating cells. There are only a few studies examining the role of Arp2/3 and formins in contact
146 guidance. Conflicting conclusions regarding the role of regulators like the Arp2/3 complex in managing
147 cell responses to contact guidance cues further complicate this landscape. While some studies suggest that
148 inhibiting Arp2/3 enhances cell alignment [36,37], others report the opposite [34]. What remains unknown is
149 the relationship between linear F-actin fibers and the enhanced contact guidance. Based on previous work,
150 it is likely that linear F-actin fibers are responsible for the stronger contact guidance, allowing cells to
151 better align and follow collagen fibrils. In contrast, branched F-actin fibers allow the cell to probe the
152 environment in many different directions and make turns and likely result in lower contact guidance.

153 In this paper, we use a fibril transfer technique to move native collagen fibrils assembled on mica
154 onto substrates with tunable stiffness. The contact guidance response of different cells with distinct
155 migration modes is explored in order to understand how cells with distinct cytoskeletal structures respond
156 differently to aligned collagen fibrils. We systematically assess how stiffness regulates contact guidance
157 and the role of myosin-mediated contraction in predicting contact guidance fidelity. We probe the balance
158 of linear and branched F-actin in determining contact guidance fidelity by assessing contact guidance
159 under both formins and Arp2/3 inhibition. Finally, we characterize a newly discovered epithelial
160 migration mode on aligned collagen fibrils. This mode of migration involves switching between parallel
161 and perpendicular migration with respect to aligned collagen fibrils. We explore the role of substrate
162 stiffness and the balance of formin-mediated linear F-actin and Arp2/3-mediated branched F-actin on
163 parallel and perpendicular migration of epithelial cells.

164 # 2. Materials and Methods:

165 **2.1 Assembling collagen on mica**

166 A freshly cleaved 15 mm x 15 mm piece of muscovite mica (highest grade VI, Ted Pella, Redding, CA)
167 was used for the epitaxial growth of collagen fibrils. Rat tail collagen type I (Corning, Corning, New
168 York) was diluted using 50 mM Tris-HCl (Fisher Scientific, Waltham, Massachusetts) and 200 mM KCl
169 (Fisher Scientific, Waltham, Massachusetts) to achieve final concentrations of 10 or 100 μg ml^{-1} and
170 added to the top of the mica. Following the 12-hour incubation period, the mica was washed with nano-
171 pure water. The mica was then placed inside a tissue culture dish, allowed to dry overnight and used the
172 following day. To prepare trimeric collagen structures on mica, 50 mM citric acid-sodium citrate (Fisher
173 Scientific) and 200 mM KCl at pH 4.3 were used to dilute the collagen, and the mica was incubated as
174 above.

175

176 **2.2 Functionalizing and transferring collagen fibrils to glass**

177 First, 22 mm × 22 mm coverslips (Corning, Corning, New York) were treated with piranha solution (3:1
178 H_2SO_4 (Fisher chemical) to H_2O_2 (Fisher chemical)) for 1 hour to ensure thorough cleaning and
179 activation. After treatment, the coverslips were immersed in 1% (v/v) 3-aminopropyltriethoxysilane
180 (APTES, Thermo scientific) solution prepared in 1 mM acetic acid (Alfa Aesarfor, Ward Hill,
181 Massachusetts) for 2 hours to facilitate silanization. The coverslips were then thoroughly rinsed with
182 deionized water and allowed to air dry. Subsequently, the coverslips were baked in an oven at 100 °C for
183 1 hour to promote covalent bonding of the APTES layer. Once cooled, the coverslips were treated with
184 6% (v/v) glutaraldehyde (Electron Microscope Science, Hatfield, Pennsylvania) in Dulbecco's Phosphate-
185 Buffered Saline (DPBS) for 2 hours to introduce aldehyde functional groups. Following this treatment,
186 the coverslips were extensively washed with deionized water to remove residual glutaraldehyde.
187 Coverslips were good for two weeks. For transferring the collagen, 30% gelatin (Sigma Aldrich, St.
188 Louis, Missouri) was dissolved in water and heated up to 40 °C for an hour, and 500 μl of the gelatin
189 solution was placed on the mica with assembled collagen. After a 1-hour incubation, the gelatin was
190 peeled off and placed on the target substrate, which was either chemically functionalized glass. Following
191 an additional hour of incubation of the gelatin on the target substrate, the samples were washed with 5 ml
192 of DPBS lacking magnesium and calcium (Gibco, Waltham, Massachusetts) by placing the DPBS inside
193 the culture dish containing the substrate and incubating at 37 °C for 2 hours. After this period, the
194 underside of the sample was cleaned with a Kim wipe (Kim wipe Kimberly-Clark, Irving, Texas), and the
195 substrate was prepared for cell seeding.

196

197 **2.3 Fabricating and transferring collagen fibrils to polyacrylamide gels**

198 First, 22 x 22 mm coverslips were thoroughly cleaned and then covered with 0.1 M NaOH for 10 minutes.
199 Following this, the coverslips were treated with a 5% APTES solution for 5 minutes. The coverslips were
200 then washed three times with deionized water, each wash lasting 5 minutes. Next, a 0.5% glutaraldehyde
201 solution was applied to the coverslips for 30 minutes, followed by additional washes with deionized
202 water. To prepare polyacrylamide gels with different elastic moduli, solutions of 3%, 5%, and 8%
203 acrylamide and 0.03%, 0.1%, and 0.26% bis-acrylamide were prepared and 0.05% Ammonium Persulfate
204 (APS, Bio-Rad, Hercules, California) and 0.15% N,N,N', N'-Tetramethylethylenediamine (TEMED,
205 Fisher Scientific), respectively, to achieve gels with elastic moduli of 200, 2000, and 20000 Pa [38].The
206 functionalized coverslips were placed face down onto drops of these solutions on microscope slides,
207 allowing polymerization to occur for 20 minutes. The samples were then treated with 2 mM Sulfo-
208 SANPAH (Thermo Scientific) under UV light for 8 minutes to functionalize their surfaces. For the
209 subsequent steps, either the fibril transfer technique was employed as described above for glass or, in the
210 case of preparing trimer samples, the coverslips were exposed to 100 μg ml^{-1} collagen dissolved in 0.01 M
211 acetic acid overnight in the fridge.
212
213 **2.4 Characterizing collagen fibrils using Atomic Force Microscope (AFM) imaging and**
214 **immunofluorescence**
215 The topography of the collagen assembly on mica and transferred to glass was imaged using an AFM
216 (Digital Instruments, now Bruker Nano, Santa Barbara, CA) multi-mode AFM in tapping-mode with
217 TESPA probes with 40 mV drive amplitude and frequency of 320 kHz. Captured images were processed
218 with the plain fit and flattened routines as appropriate. Collagen fibrils were also stained and imaged
219 using immunofluorescence. Collagen fibril samples were first blocked with blocking buffer (0.02 g ml^{-1}
220 BSA prepared in 10% TBS containing 0.01% Tween-20) for 20 minutes and then incubated with 1:100
221 collagen antibody (polyclonal rabbit, Thermo fisher, Bio-Rad-2150-1908) for 24 hours. After washing
222 three times with 1x TBS for 5 minutes each, samples were incubated with a 1:200 dilution of donkey anti-
223 rabbit 488 (Jackson Immuno Research, #711-035-152) secondary antibody for 1 h, followed by additional
224 washes.
225
226 **2.5 Culturing cells and treating with inhibitors**
227 An immortalized human foreskin fibroblast cell line (HFF, ATCC, Manassas, VA), a human mammary
228 carcinoma cell line (MDA-MB-231, ATCC), a metastatic human melanoma cell line (WM-266-4,
229 ATCC), an immortalized human keratinocyte cell line (HaCaT, kind gift from Dr. Torsten Wittmann) and
230 an immortalized monocyte cell line (THP-1, ATCC) were used. MDA-MB-231s, WM-266-4 and HaCaTs
231 were cultured in Dulbecco's modified Eagles medium (DMEM, Sigma Aldrich). It was supplemented

232 with 10% fetal bovine serum (FBS) (Gibco, Grand Island, New York, USA), 1% penicillin–streptomycin
233 (Gibco), and 1% Glutamax (Gibco) at 37 °C in 5% CO_2. The same media with 15% FBS (Gibco) was
234 used for culturing HFF cells. THP-1 cells were cultured in RPMI-1640 media with 10% FBS, 1%
235 Penstrep, 0.05 mM BME (β-Mercaptoethanol). When live cells were imaged, cells were placed in culture
236 media Dulbecco's Modified Eagle Medium that lacked phenol red, but contained 15 mM 4-2-
237 hydroxyethyl) piperazine-1-ethanesulfonic acid (HEPES), 1x Glutamax, 1x penicillin/streptomycin, 10%
238 Fetal bovine serum (FBS). For inhibitor treatments, cells were centrifuged, counted and suspended in
239 culture media. SMIFH2 (Millipore), CK-666 (Millipore) and blebbistatin (Millipore) were dissolved at 50
240 mM, 50 mM and 20 mM stock solutions in dimethyl sulfoxide (DMSO). Stock solutions of the inhibitor
241 were diluted in either culture media or imaging media by at least 1000-fold to make working solutions of
242 0.5, 5, 10, 20, and 50 mM. For the control group, 0.1% DMSO was added to cell culture media or imaging
243 media.
244
245 **2.6 Immunofluorescence imaging and analyses**
246 Cells were plated onto target substrates at concentration of 20,000 cells ml^{-1} for subsequent experiments.
247 Cells were fixed and stained to visualize their F-actin structure and quantify their response to contact
248 guidance through morphology and alignment behavior. First, the cells were treated with 4%
249 paraformaldehyde (Fisher Scientific) for 10 minutes, prepared by diluting 16% paraformaldehyde in a
250 cytoskeleton buffer consisting of 10 mM 2-N-morpholino ethane sulfonic acid (MES, pH 6.1, Fisher
251 Scientific), 3 mM $MgCl_2$ (Fisher Scientific), 138 mM KCl (Fisher Scientific), and 2 mM EGTA (Sigma
252 Aldrich). Next, cells were permeabilized using a 0.5% Triton-X (Fisher Bioreagents) solution in the
253 cytoskeletal buffer for 5 minutes. Unreacted aldehydes were then blocked with 100 mM glycine (Fisher
254 Scientific) for 15 minutes. Cells were washed three times with 1x Tris Buffered Saline (TBS) for 5
255 minutes each. Cells were stained with Alexa 488-phalloidin (Thermo Fisher Scientific) for 1 hour and
256 DAPI (Sigma) for 15-30 minutes in 1x TBS containing 0.1% (v/v) Tween-20 (Fisher Bioreagent) and 2%
257 (w/v) Bovine Serum Albumin (BSA, Sigma Life Science). For phospho-myosin and anti-paxillin staining,
258 after initial phalloidin staining and washing with 1x TBS, cells were incubated with 1:50 dilution of
259 phospho-myosin antibody (Cell Signaling, mouse, 3675) or a 1:200 dilution of anti-paxillin primary
260 antibody (BD Biosciences, mouse, 610051) for 24 hours at 4 °C. Samples were then washed with 1x TBS,
261 followed by incubation with a 1:200 dilution of donkey anti-mouse IgG secondary antibody (Jackson
262 ImmunoResearch, 715-175-150) and 1:500 dilution of DAPI for 1 hour. Samples were washed again with
263 1x TBS three times for 5 minutes each. To improve image resolution, Prolong Gold mounting media
264 (Thermo Fisher) was applied between the substrate with cells and the cover slides. Samples were sealed
265 with VALAP (a mixture of Vaseline, lanolin, and paraffin) and imaged the next day using epifluorescence

266 microscopy with 10x, 40x, and 60x objectives (*NA* = 0.3, *NA* = 1.3, and *NA* = 1.49, Nikon). The
267 immunofluorescence images were analyzed with ImageJ. Lines around the cell's edge were drawn and an
268 oval was fit to the cell shape. The aspect ratio was calculated as the ratio of the major axis of the cell
269 divided by the minor axis of the cell. The angle of the cell was calculated as the angle between the long
270 axis of the cells and the horizontal vector of the image. To quantify the directionality of fixed cells, the
271 migration vector was analyzed using Python. The Directionality Index (DI) was calculated as the
272 $\cos(2|\Delta\theta|)$, where $|\Delta\theta|$ represents the angular deviation of the cell from the average cell angle in the
273 region. Cells with an area less than 300 μm^2 and an aspect ratio less than 1.5 were assigned a random
274 number for their angle to calculate the average angle of the region as their specific direction was not
275 readily calculatable. Then we used that angle to calculate a DI for all cells. If the area was less than 300
276 μm^2 then the DI was not included in the calculation. However, for THP-1 cells, which are small and do
277 not spread, applying a threshold of 300 μm^2 results in the exclusion of almost all data. Therefore, we
278 included all data points in the calculation of the DI for THP-1 cells. For the calculation of area and aspect
279 ratio, all cells were included.
280
281 **2.7 Western blotting**
282 We employed Western blotting to quantify phosphorylated myosin expression across different cell lines.
283 Using two million cells from different mammalian cell lines (HFF, HaCaT, MDA-MB-231, WM-266-4,
284 and THP-1 cells) at an approximate confluency of 80% in a cell culture dish, cells are washed with 1x
285 PBS and trypsinized, counted and centrifuged in a conical tube to form a pellet. A total of 100 µl of 1x
286 sample buffer was added to the tube. The cells in the tube were lysed on ice with a conical pestle to
287 ensure cells formed a uniform lysate. Protein lysate was heated at 94 °C for 5 minutes. Proteins were
288 separated on 4-20% precast polyacrylamide gel (Bio-Rad, Min-PROTEAN® TGX Stain-Free™ Protein
289 Gels, 10 well, 30 µl, 4568093) by loading a total of approximately 90 µg of protein lysate for each cell
290 line in the gel wells, running the gel at 120 V for 1 hour and transferring it onto a polyvinylidene
291 difluoride (PVDF) transfer membrane (Thermo-Fisher Scientific, PB9220) at 100 V for 1 hour and 30
292 minutes. The blot was blocked in PBST, and 5% skim dried nonfat milk at 37 °C for 1 hour. The
293 membrane was incubated in primary phospho-myosin antibody (Cell Signaling, mouse, 3675, 1:200
294 dilution) and or β-actin antibody (Santa Cruz, mouse, C-2, sc-8432, 1:500 dilution). Antibodies were
295 incubated at 4 °C overnight, washed using washing buffer three times for 5 minutes, followed by
296 treatment with donkey anti-mouse secondary antibody (Jackson ImmunoResearch, 715-035-150, 1:500)
297 incubated for 1 hour, then the membrane was rewashed three times for 5 minutes. Blots were developed
298 using freshly prepared enhanced chemiluminescent (ECL) reagents (250 mM luminol in DMSO, 90 mM p-
299 coumaric in DMSO acid,1 M Tris-HCI pH 8.5, 30% H_2O_2 and water) and visualized using Bio-Rad Gel

300 Doc XR+ Imaging system. Lastly, to quantify the protein bands, we used Image J software. Band
301 intensities on the immunoblot were quantified by selecting a rectangular region of interest around the
302 band as well as one around a background region locally. The intensity of the background region was
303 subtracted from the intensity of the band region. This value was divided by the corresponding background
304 subtracted value for β-actin as a loading control.
305
306 **2.8 Quantifying gel compaction**
307 For the gel compaction experiment, cells were embedded in a 2 mg ml^{-1} or 1.5 mg ml^{-1} collagen gel,
308 where the optimum percentage of DMEM and FBS were maintained depending on specific cell lines. To
309 achieve that, a solution of 5x DMEM, 10x FBS, and 10^7 cells ml^{-1} mixture was used to achieve a final
310 percentage of 1x DMEM, 10 or 15% FBS, and concentration of cells corresponding to each cell line
311 mentioned above. To neutralize the acidic collagen gel compaction mixture, 0.1 M filter sterile NaOH was
312 employed. Finally, filter-sterilized deionized water was used to attain a total volume of 500 µl collagen
313 gel compaction mixture. After thoroughly mixing the collagen gel compaction mixture by avoiding air
314 bubble formation, the mixture was put into a pre-sterilized cylinder shaper placed in a 6-well dish. Then
315 the gel was incubated for 2 hours at 37 °C for gel formation, the cylinder shaper was removed and 2 ml of
316 corresponding cell culture media was added to the gel to produce a floating gel in media. Gel images were
317 taken at 0, 4, 20, 32, 54, 72, 96, 132, and 140 hours to observe the change in gel diameter. For the
318 SMIFH2 and CK-666 inhibitor-treated gel compaction experiments, final concentrations of 20 and 50 µM
319 SMIFH2 and 5 and 25 µM CK-666 were achieved within both collagen gel and media around the gel to
320 avoid concentration differences due to diffusion. Obtained images were analyzed in ImageJ to measure
321 the gel diameter at different times corresponding to the degree of compaction. The gel diameter at
322 different time points was analyzed using GraphPad Prism 8, where non-linear regression analysis for a
323 two-phase decay model was performed. To determine the fractional compaction, the gel diameter at 48
324 hours for each replicate was calculated using the two-phase decay equation. The fractional compaction is
325 then defined as the ratio of the change in diameter from 0 hours to 48 hours, relative to the diameter at 0
326 hours.
327
328 **2.9 Live cell migration imaging and analyses**
329 Chambers were fabricated by cutting adhesive heat resistant thin transparent silicone rubber sheets using a
330 craft cutter to form a chamber on a glass surface. This chamber is filled with clear media, supplemented
331 with 10-15% FBS, depending on the cell line. Once the media is prepared, the substrate with the cells is
332 flipped over onto the chamber. The chamber is sealed with VALAP. The setup is then imaged over an 8-
333 hour period with images captured at 2-minute intervals. This allows for detailed observation and analysis

of cell migration behavior. The DI calculations for live cell migration were based on the average of $\cos(2|\Delta\theta|)$, with $|\Delta\theta|$ being the angle difference between the fibrils and the cell's direction, derived from changes in x and y positions at 2-minutes intervals and averaged over 8 hours. Speed was calculated by averaging the displacements measured every 2 minutes, dividing the total displacement over the 2 minutes by the corresponding time interval, and then averaging the resulting speeds over 8 hours. To categorize migration direction during live cell migration, the direction of cell movement was calculated over a 12 minute window every six 6 minutes. The number of steps was classified based on deviation angles: less than 30°, between 30° and 60°, and greater than 60°, using R for analysis. Steps with speeds less than 10 μm/hour were considered slow.

2.10 Assessing statistical significance

Statistical significance was assessed using a 95% confidence interval, calculated from the experimental data and placed on graphs in the form of error bars. Nonoverlapping confidence intervals indicate statistical significance to approximately $p < 0.05$.

3. Results:

3.1 Self-assembled collagen fibrils transferred to glass induce robust fibroblast alignment

Collagen fibrils can be epitaxially assembled on mica via electrostatic interactions between the collagen fibrils and the mica. Under specific buffer conditions which include collagen concentration and adsorption time, well-aligned collagen fibrils can be formed and imaged using AFM. Ultrastructural characteristics like D-banding as observed *in vivo* are formed (**Figure 1A**). We have previously shown collagen fibril alignment across large swaths of the substrate [18]. Similar collagen fibril structure can be seen on the transferred substrates as imaged by immunofluorescence (**Supplementary Figure 1**). While the collagen intensity after transfer was higher than that on mica, this is likely due to residual gelatin left after transfer that can be recognized by the collagen antibody. Collagen level is similar on all transferred substrates indicating similar transfer efficiency (**Supplementary Figure 1**). Human foreskin fibroblasts (HFFs) readily align and migrate along the collagen fibrils (**Figure 1A&B**). However, because of their contractile nature, they pull the collagen fibrils from the mica substrate after about 1 hour, culminating in complete collagen fibril delamination at around 4 hours (**Figure 1A&B**). This catastrophic delamination timing is cell density-dependent, occurring at different times across the substrate, leading to high variability in the fraction of cells that remain at 4 h (**Figure 1B**). We assessed whether delamination occurred on other substrates. We adsorbed collagen trimers (t) to mica using low pH, assembled aligned collagen fibrils (af) on mica, created multi-directional collagen fibrils (mdf) by using higher collagen concentrations and transferred aligned collagen fibrils (tf) to functionalized glass. AFM images verified that the solution conditions and transfer approach created the desired fibril morphologies (**Figure 1C**). Cell alignment was quantified using a directionality index. The directionality index was calculated by finding the deviation of the individual cell alignment direction with respect to the average cell alignment direction within one image and using this angle in the directionality index calculation as outlined in the materials and methods. Directionality index values of 1 indicate high alignment with collagen and high-fidelity contact guidance and values of 0 indicate low alignment with collagen and low contact guidance fidelity. HFFs were not well spread or aligned on trimers (**Figure 1D**). On aligned collagen fibrils assembled on mica, cells were aligned well initially (1 hour), but eventually detached due to collagen delamination (4 hours), leaving both large clusters as well as a small number of single cells that were not well aligned (**Figure 1E**). Multi-directional collagen fibrils induced better spreading than the trimers, but the cell appeared confused and directional alignment was poor. Transferred collagen fibrils resulted in robust spreading and alignment of HFFs due to the chemical linkage of the collagen fibrils to the glass surface. Consequently, HFFs, mesenchymal cells that are known to be highly contractile cells engage in robust contact guidance on aligned collagen fibrils, but not on other non-aligned collagen substrates. Furthermore, collagen delamination and deadhesion of cells only occurs on aligned collagen fibrils

assembled on mica. Consequently, long-term HFF alignment is only observed on collagen fibrils transferred to glass (**Figure 1E**).

3.2 Optimal contact guidance occurs at different stiffnesses depending on the cell type

Given that HFFs robustly spread and orient on aligned collagen fibrils, but only when collagen fibril delamination was blocked by transferring collagen fibrils to glass, we examined whether this behavior was observed in other cell lines. Previously, we showed that carcinoma cells that adopt a mesenchymal mode of migration (MDA-MB-231) tended to robustly orient and directionally migrate on aligned collagen fibrils, whereas carcinoma cells that adopt an amoeboid mode of migration (MTLn3) did not [18,19]. Along with HFF and MDA-MB-231 cells, we examined WM-266-4, HaCaT, and THP-1 cells. WM-266-4 cells are a mesenchymal to amoeboid mode-switching cell line.[31] HaCaTs migrate as epithelial cells. THP-1 cells are a model naive immune cell that moves with an amoeboid migration mode. We examined the orientation of individual cells across different cell lines on collagen fibrils assembled on mica as well as those transferred to glass (**Figure 2A**). The delamination of collagen fibrils assembled on mica was observed in response to HFF (**Figure 1**) or MDA-MB-231 [20] cells that is blocked when collagen fibrils are transferred to glass. This suggests that the perceived stiffness that the cell experiences is lower on fibrils adsorbed to mica compared to those transferred to glass and that this might control the cell response to aligned collagen fibrils. HFF and MDA-MB-231 cells adopted extended, large area morphologies with long stress fibers in the direction of the long axis of the cell, typical of mesenchymal cells. However, HFF cells had a wider body and more pronounced F-actin stress fibrils within and paxillin focal adhesions underneath the cell body (**Figure 2B**). WM-266-4 and HaCaT cells adopted an epithelial cell morphology with numerous different types of F-actin fibrils including longitudinal stress fibers and transverse arcs that terminated in large focal adhesions (**Figure 2B**). Finally, THP-1 cells were not well spread, did not include well-defined F-actin fibers and only had small focal adhesions (**Figure 2B**). HFF cells spread to the greatest extent and adopted spread areas roughly 4-fold larger than any of the other cell lines. Interestingly, the spread area did not differ dramatically between aligned collagen fibrils assembled on mica and those transferred to glass except for HFFs and HaCaTs, where areas for both cell lines were larger when the collagen fibrils were transferred to the stiff glass substrate (**Figure 2C**). The degree of directional alignment differed dramatically across the cell lines. HFF and MDA-MB-231 cells robustly oriented on aligned collagen fibrils, whether the collagen fibrils were assembled on mica or transferred to glass (**Figure 2D**). WM-266-4 cells oriented well on aligned collagen fibrils assembled on mica, but poorly on those transferred to glass. HaCaTs adopted an intermediate degree of orientation, whereas THP-1 cells adopted a poor degree of orientation on aligned collagen fibrils. Both HaCaTs and THP-1s did not show differences across the two substrates. The trends in aspect ratio were similar to

416 those in directionality index, indicating that aspect ratio is a reasonable proxy for contact guidance ability
417 (**Supplementary Figure 2**). Consequently, mesenchymal cells were best at orienting on aligned collagen
418 fibrils, followed by cells that adopt an epithelial morphology. Amoeboid cells were worst at orienting on
419 aligned collagen fibrils. Furthermore, there are substrate-specific differences in responses to aligned
420 collagen. HFFs and HaCaTs were better spread on the stiff substrate (glass), whereas MDA-MB-231 and
421 WM-266-4 cells were better aligned on the soft substrate (mica).
422 Given that some cell lines directionally migrate better on collagen fibrils chemically attached to
423 stiff glass substrates, while others prefer collagen fibrils that are loosely attached to mica, we explored the
424 role of both external mechanical properties of the substrate and internal contractile force generation
425 properties of the cell lines. Many of the cell lines showed measurable, but modest dependence of
426 directionality on stiffness, except for WM-266-4 cells, which showed a large and steadily declining
427 directionality for increasing stiffness (**Figure 3A**). We observed a different stiffness for maximal
428 directional alignment across the cell lines. HFFs appeared to align best on 0.2 kPa, MDA-MB-231 and
429 WM-266-4 cells aligned best on mica and HaCaTs aligned best on 2 kPa. The poor directionality of THP-
430 1 cells hindered determining the stiffness of optimal directional migration. Areas and aspect ratios were
431 roughly the same for the cells across stiffnesses, except for HFFs and HaCaTs, which showed robust
432 increases in area as stiffness increased (**Supplementary Figure 3A-C**). Studies have indicated a
433 correlation between directionality and internal cell contractile force, which is associated with myosin
434 activity, a motor protein in cells [8,12,19,39,40]. We hypothesized that cells with higher directionality would
435 exhibit higher levels of phosphorylated myosin (p-Myo). Initially, we considered fibril patterns that test
436 this hypothesis and measured phosphorylated myosin immunofluorescence. Interestingly, cells with
437 roughly similar shapes showed variability in phosphorylated myosin level (**Figure 3B**). Also, conditions
438 that produced the highest directionality had the lowest phosphorylation level (mica) (**Figure 3C**). This
439 differed somewhat from cells on a non-directional collagen cue (collagen trimers on glass), where there
440 appeared to be an increase in phosphorylated myosin as has been seen previously. Cells plated on
441 collagen trimers attached to 0.2 kPa PAA (Polyacrylamide) gel were essentially unspread and showed
442 extremely high signal. However, it is important to note that high phosphorylated myosin level is only
443 efficacious if coincident with a contractile F-actin structure and adhesion to the substrate. Challenges in
444 accurate quantification of immunofluorescence images led to our assessing myosin phosphorylation and
445 contraction by two different means: western blotting and collagen gel compaction. Interestingly, the
446 maximal directionality for each cell type correlated well with the phosphorylated myosin level as
447 measured by western blot (**Figure 3D and Supplementary Figure 3E**). To further assess contractility,
448 we conducted a compaction test. Cells compact collagen gels at different rates (**Supplementary Figure**
449 **3D**). The fractional compaction can be defined as the ratio of gel diameter change relative to the initial

450 diameter over 48 hours. The results showed that HFF and MDA-MB-231 cells, both exhibiting
451 mesenchymal migration with the highest directionality, had the highest fractional compaction (**Figure**
452 **3E**). HaCaTs showed lower compaction, followed and WM-266-4 and THP-1 which did not compact
453 gels. Consequently, the directionality of cells was both stiffness and cell type dependent. In addition,
454 contact guidance ability correlated strongly with both phosphorylated myosin as measured by western
455 blot and fractional compaction, two measures of the ability of cells to generate and transmit contractile
456 force.
457
458 **3.3 Formins regulate cell migration parallel to aligned collagen fibrils, while Arp2/3 controls**
459 **movement perpendicular to collagen fibrils**
460 In order to explore why different cells on different substrates engage in contact guidance to different
461 extents, we perturbed the F-actin cytoskeleton. Different cells use unique F-actin regulatory machinery to
462 form a particular cell shape and migrate with a particular mode. Two important classes of F-actin
463 regulatory proteins are Arp2/3 and the formins family of F-actin regulators. Arp2/3 forms branched F-
464 actin, whereas formins regulate the formation of linear F-actin. Broad lamellipodia formed by branched F-
465 actin networks likely give the cell the ability to make turns during migration, whereas aligned stress
466 fibrils have been found to be important in contact guidance [19]. In addition, branched F-actin and linear F-
467 actin draw G-actin from the same pool, creating a tempting hypothesis that when one type of network is
468 diminished, the cell can build the other type of network [41]. Consequently, we hypothesized that these F-
469 actin regulators control contact guidance in distinct ways. To test this hypothesis, we employed
470 pharmacological agents including SMIFH2, a formin inhibitor, and CK-666, an Arp2/3 inhibitor.
471 Inhibition of formins with SMIFH2 in HFF and MDA-MB-231 cells, resulted in dramatic
472 morphology changes (**Figure 4A**). Cells were smaller (**Supplementary Figure 4A&B**) and had
473 diminished stress fiber formation and smooth edges suggestive of branched F-actin networks. Similar
474 morphological responses were seen on both aligned collagen fibrils on mica and aligned collagen fibrils
475 transferred to glass. In addition, cells treated with SMIFH2 showed marked decrease in directionality
476 (**Figure 4B&C**) and aspect ratio (**Supplementary Figure 4C&D**) at high concentrations. The decrease in
477 directionality of cells plated on aligned collagen fibrils transferred to glass is small, but measurable at 20
478 μM, increasing through 50 μM, whereas cells plated on aligned collagen fibrils assembled on mica seems
479 to require higher SMIFH2 concentrations to achieve measurable changes in directionality. Given the
480 correlation observed between directionality and contractility and that SMIFH2 is known to block myosin
481 activity at high concentrations (> 50 μM) [42], we measured contractility in two different ways. First, we
482 plated cells on collagen fibrils assembled on mica with and without 20 μM SMIFH2 and measured the
483 kinetics of fibril delamination (**Figure 4D**). There was a small increase in fraction of cells remaining, but

484 it was not statistically significant. This suggests that contractility at this concentration was not
485 dramatically inhibited. Compaction kinetics showed a different response (**Supplementary Figure 4E**).
486 Both 20 and 50 μM diminished compaction as compared to untreated cells (**Figure 4E**). Consequently,
487 inhibiting formins diminishes stress fibril formation and modestly diminishes directionality at
488 concentrations that likely do not affect myosin activity. At higher formins inhibitor concentrations,
489 myosin is likely inhibited, resulting in dramatic alterations in directionality as we have demonstrated
490 previously [43]. Interestingly, formin inhibition more robustly affects compaction, even at low
491 concentrations. This indicates that formin-mediated F-actin cytoskeletal structures contributes to contact
492 guidance.
493 Given that linear F-actin fibrils facilitated by formin activity enhance directionality during contact
494 guidance, we were interested in assessing the role of Arp2/3-mediated branched F-actin networks in
495 contact guidance. Inhibition of Arp2/3 with CK-666 in HFFs resulted in very few morphological changes
496 (**Figure 5A**). However, treatment with CK-666 resulted in increased directionality compared to control
497 cells, indicating that Arp2/3 activation inhibits contact guidance (**Figure 5B**). We assessed whether
498 Arp2/3 inhibition could affect the cells ability to delaminate collagen fibrils. It did not, suggesting myosin
499 activity was not greatly altered (**Figure 5C**). Additionally, inhibiting Arp2/3 showed only a small
500 decrease in gel compaction (**Figure 5D** and **Supplementary Figure 5**). Even if Arp2/3 inhibition were to
501 affect compaction through diminishing myosin contractility, the known effect on contact guidance in
502 response to diminished myosin contraction would have been to diminish contact guidance. However, this
503 was not the case as there was a measurable increase in directionality under Arp2/3 inhibition.
504 Consequently, Arp2/3 likely acts to inhibit contact guidance through the production of branched F-actin
505 networks that give cells an ability to change directions by partially ignoring contact guidance cues. Taken
506 together with data above, formins enhances contact guidance whereas Arp2/3 diminishes contact
507 guidance.
508
509 **3.4 The switch-like directional migration behavior of HaCaT cells can be modulated by**
510 **manipulating both formins and Arp2/3**
511 We have previously established that mesenchymal cells robustly engage in contact guidance on aligned
512 collagen fibrils. Epithelial cells on the other hand seem to be less robust in their alignment (**Figure 2 &**
513 **3**). Consequently, they may be a better model system by which to assess whether formins or Arp2/3
514 inhibition can increase or decrease cell alignment. However, it is difficult to determine the direction of
515 HaCaT cell migration in fixed images, due to the fact that they are less aligned than mesenchymal cells.
516 Consequently, we examined HaCaT migration on aligned collagen fibrils assembled on mica (low
517 stiffness) or transferred to 2 kPa PAA gel (moderate stiffness) or glass (high stiffness). Montages of live

518 cell migration showing images at 0, 2, 4, and 8 hours on these substrates revealed interesting behavior
519 (**Figure 6A**). Unlike mesenchymal cells which migrate solely parallel to collagen fibril alignment [18,19],
520 HaCaT cells migrated both parallel to the collagen fibrils as well as perpendicular to collagen fibrils,
521 exhibiting a switching behavior (**Figure 6A**). Both parallel and perpendicular movement additionally
522 complicates interpretation of contact guidance from fixed cells. Consequently, we assessed migration
523 directionality on these different substrates. Indeed, directionality was lower on both collagen fibrils
524 assembled on mica and those transferred to 2 kPa PAA when measured by migration as compared to
525 morphology (**Figure 6B**). Directionality index increased with substrate stiffness, progressing from mica
526 to glass (**Figure 6B**). Interestingly, cell speed exhibited an inverse trend (**Figure 6C**), demonstrating that
527 stiffer substrates slow down cell migration but enhance its directedness. In order to understand the reason
528 for changes in directionality, given migration both parallel and perpendicular to collagen alignment, we
529 measured the residence time that a cell remains in either in parallel (migration angle < 30° with respect to
530 the aligned fibril direction) or perpendicular (migration angle > 60° with respect to the aligned fibril
531 direction) movement. While HaCaT cells spend more time migrating parallel to the collagen fibrils, they
532 do spend a considerable amount of time migrating perpendicularly (**Figure 6D**). HaCaT cells spend more
533 time in parallel movement on stiffer substrates (collagen fibrils transferred to glass) than on softer
534 substrates (collagen fibrils assembled on mica). This agrees with the data showing that HaCaT cells
535 migrating on collagen fibrils transferred to glass have a higher directionality index. In addition to
536 residence time, we quantified the fraction of the time cells migrate in a parallel or perpendicular manner
537 with respect to the fibrils with a more stringent criterion. Migration parallel to fibril direction was defined
538 as a migration angle < 30° with respect to the aligned fibril direction, whereas migration perpendicular to
539 fibril direction was defined as a migration angle > 60° with respect to the aligned fibril direction (**Figure**
540 **6E**). Increased stiffness diminished perpendicular movement compared to parallel movement, but
541 migration on the 2 kPa PAA substrate showed the most evenly balanced parallel and perpendicular
542 movement. Consequently, unlike mesenchymal cells, epithelial cells have two modes of directed
543 migration on aligned collagen fibrils, one that is parallel and one that is perpendicular. Furthermore, the
544 stiffness of the underlying substrate can tune the dominance of one of these modes of migration over the
545 other.

546 Given that HaCaT cells have intermediate directionality and that they have both parallel and
547 perpendicular movement, we were interested in assessing the role of formins and Arp2/3 in controlling
548 directionality and the balance of these different directional migration modes. As demonstrated in the
549 previous section, formins enhance directionality, whereas Arp2/3 diminishes directionality. A hypothesis
550 that flows from this observation is that formins enhance parallel movement, whereas Arp2/3 enhances
551 perpendicular movement. We fixed HaCaTs plated on aligned collagen fibrils transferred to glass after

552 formins or Arp2/3 inhibition (**Figure 7A**). Inhibiting formins results in larger cells that seem to be
553 directionally confused, whereas inhibiting Arp2/3 results in a similar morphology as compared to control
554 with only modest directional confusion. To complement fixed cell morphology, HaCaTs were imaged
555 during migration. Montages are shown containing images at 0, 2, 4, and 8 hours (**Figure 7B**). As
556 described in Figure 7A, formin inhibition appears to enhance cell area and both formin and Arp2/3
557 inhibition seem to increase directional confusion and cell migration speed (**Figure 7B**). We quantified
558 directionality index and speed. Directionality index assessed by fixed cells and in live cells decreased
559 robustly when formins were inhibited as we described above (**Figure 7C**). Inhibition of Arp2/3 only
560 modestly reduced directionality (**Figure 7C**). Speed showed a different response. Cells under formin or
561 Arp2/3 inhibition moved at the same rate as each other as well as faster than controls (**Figure 7D**). Since
562 HaCaT cells move in both parallel and perpendicular fashions, we assessed whether inhibiting formins or
563 Arp2/3 differentially affected these different directional modes of migration. Similar to our previous
564 analyses (**Figure 6**), we quantified and analyzed cell movements to evaluate the effects of formins or
565 Arp2/3 inhibitors. Decreases in residence time (**Figure 7E**) tracked with changes in directionality index
566 (**Figure 7C**). For cells treated with the Arp2/3 inhibitor (25 μM CK-666), we observed an increase in both
567 parallel and perpendicular steps (**Figure7F**), resulting in a slightly lower directionality index, compared
568 to the control due to the balanced distribution between parallel and perpendicular movements (**Figure**
569 **7C**). In contrast, cells treated with the formin inhibitor (20 μM SMIFH2) showed a similar fraction of
570 parallel steps compared to the control but an increased fraction of perpendicular movements, resulting in a
571 markedly lower directionality than the control. These results for epithelial cells agree with the above
572 results for mesenchymal cells. Formins tend to enhance parallel migration of epithelial cells, whereas
573 Arp2/3 has more subtle effects, including diminishing the fraction of parallel moving cells.
574 To further establish that the formin inhibitor was not simply blocking myosin activity indirectly
575 to alter contact guidance, we investigated the role of myosin contractility in contact guidance by
576 perturbing contractility using blebbistatin (bleb). Blocking myosin diminished directionality and
577 increased cell speed (**Supplementary Figure 7B&C**), consequences that we have described in
578 mesenchymal cells elsewhere [19]. Interestingly, when assessing various concentrations of SMIFH2, a
579 notable trend emerged. At 10 μM SMIFH2, the directionality index exhibited a significant increase,
580 approaching control levels (**Supplementary Figure 8**). This behavior was also observed in live cell
581 migration analyses (**Figure 8**), where the directionality index for 10 μM SMIFH2 was closer to the control
582 than the 20 μM SMIFH2 condition. To explore whether diminished myosin activity explained the decrease
583 in directionality index and increase in speed moving from 10 μM SMIFH2 to 20 μM SMIFH2, we treated
584 cells with both 10 μM SMIFH2 and 3 μM blebbistatin. This did not diminish directionality index to the
585 same extent as either 3 μM blebbistatin or 20 μM SMIFH2 alone. This indicates that the formin inhibitor is

586 uniquely affecting contact guidance and does not simply act as a myosin inhibitor. All inhibitor
587 conditions for HaCaTs were then plotted on the same speed and directionality index graph. Interestingly,
588 a biphasic response is seen, whereby speed increases dramatically, when directionality index is somewhat
589 diminished, but when directionality index highly diminished speed decreases (**Figure 8**). This indicates
590 that there is a coupling between how fast cells move and how directional they are and these parameters
591 are not independently controlled through the myosin/formin/Arp2/3 pathways. In summary, our findings
592 highlight the significant roles of formins and Arp2/3 in regulating contact guidance that are distinct from
593 myosin.

4. Discussion:

We show in this paper that contact guidance fidelity is strongly cell type dependent, where mesenchymal cells contact guide with high fidelity, epithelial cells contact guide with intermediate fidelity and amoeboid cells essentially ignore the contact guidance cue. Others have shown that there are cell type differences in response to contact guidance cues [26–29]. Broadly, these results match what we observe. Fibroblasts and more mesenchymal cells contact guide best, followed by epithelial cells, followed by amoeboid cells. However, many of these previous reports have been conducted on grooves and only specific groove characteristics result in cell-type differences. We have previously shown that aligned collagen fibrils assembled on mica reveal contact guidance differences across cells that are masked in systems like grooves or microcontact printed lines [19]. Furthermore, many of the substrates used to tease out cell type differences were very stiff and the role of stiffness on tuning the contact guidance of different cells was not explored except in one report [29].

In addition to broadly observable cell type differences contact guidance, we demonstrate that stiffness for optimal contact guidance is different for different cell types. Highly contractile cells like HFFs engage in contact guidance that is independent of stiffness. Similarly, amoeboid cell (THP-1) contact guidance is also unaffected by the underlying substrate stiffness. Only cells with intermediate contractile behavior, including MDA-MB-231, WM-266-4 and HaCaT cells show noticeable maxima in directionality index, whereas less contractile cells show optimal contact guidance on stiffer substrates. Substrate stiffness is an appreciated modulator of cell function and likely tunes contact guidance fidelity due to overlapping intracellular mechanisms [44,45]. Previously, we showed subtle differences when the underlying substrate stiffness was altered, but these were only explored in the mesenchymal MDA-MB-231 cells and amoeboid MTLn3 cells [20]. The literature shows conflicting reports examining contact guidance in MDA-MB-231 cells on flexible grooves. One report indicated that increased stiffness diminishes the cell aspect ratio [34], suggesting that that contact guidance decreases under stiffer conditions, however another report showed increased elongation and small increases in cell alignment in both MDA-MB-231 cells as well as a more epithelial-like cell line, T47D cells when stiffness was increased [29]. We showed decreases in MDA-MB-231 cell contact guidance in 3D environments after collagen crosslinking leading to increases in stiffness [12], matching what we observed on aligned fibrils in 2D here, suggesting again that the aligned collagen fibril assembled system mimics 3D environments and provides clarity with respect to discrepancies observed when using groove systems. Strengthening this argument is evidence indicating that fibril recruitment, a feature in our system and one that is particularly important soft environments dramatically enhances contact guidance [46]. Interestingly, two reports using fibroblasts and not MDA-MB-231 cells in 3D environments showed that increases in stiffness increase fibroblast contact guidance only modestly,[11,47]. It is not surprising that different cells respond differently

628 to contact guidance cues and that the response is stiffness-dependent. Fibroblasts must remodel the ECM
629 while moving along fibrils during wound healing. Since stiffness changes dramatically during the wound
630 process, but fibroblasts must continue to contact guide and generate traction force, they may need to be
631 less sensitive to stiffness cues. Similarly, for amoeboid cells, which must randomly sample the wound
632 environment, it might be important for them to ignore the directional cue. Indeed, aligned collagen fibrils
633 in the tumor microenvironment do not seem to affect T-cell infiltration [23]. Consequently, tissue
634 environments with different stiffness are likely to control cells with unique functions differently.
635 Other interesting behaviors emerged when examining cancer cell-specific responses. Indeed, the
636 ability of cancer cells to engage in contact guidance correlates with their migration mode. A recent paper
637 has shown that the strongest response to contact guidance cues occurs in cells that have processed through
638 the epithelial-to-mesenchymal transition (EMT), followed by epithelial cells, while amoeboid cells
639 showed the weakest fidelity to these cues, matching our observations [28,32]. However, our results indicate
640 that cancer cells, MDA-MB-231 and WM-266-4 cells, show dramatically increased contact guidance
641 responses on aligned collagen assembled on mica versus aligned collagen transferred to glass. This is in
642 contrast to non-transformed cells [11,29], which show only a small difference in contact guidance fidelity
643 when the stiffness of the substrate is changed. We do observe that cancer cells are more sensitive to
644 stiffness differences, decreasing their contact guidance on flexible substrates as stiffness increases.
645 However, aligned collagen fibrils assembled on mica do seem to have a unique capability to align cells
646 even in comparison to aligned collagen fibrils transferred to flexible substrates. As mentioned above,
647 fibril recruitment to the cell periphery is inhibited even when collagen fibrils are transferred to soft 200 Pa
648 substrates. Free fibers that can be remodeled and recruited to the cell periphery likely amplify the signal
649 for contact guidance [20,46]. Our work strengthens the argument that for contact guidance, specific cancer-
650 related pathways sensitize cancer cells to stiffness in comparison to non-transformed cells. It is known
651 that cancer cells have distinct mechano-sensitivity when compared to non-transformed cells [48]. This
652 includes upregulation and expression of mechanosensitive proteins such as Piezo1 [49] as well as the
653 ability of cancer cells to avoid death and resist inhibitor treatment on soft substrates [50] or alter
654 metabolism based on the mechanical properties of the ECM [51]. This differential contact guidance
655 sensitivity to substrate stiffness is yet another differentially regulated mechanical behavior in cancer cells.
656 We also demonstrate that intracellular contractility is a dominant predictor of contact guidance
657 behavior. Both myosin phosphorylation and compaction assays revealed a strong correlation between
658 increased directionality index and elevated contractility. Interestingly, the only dramatic difference
659 between compaction and myosin phosphorylation levels was WM-266-4 cells. It seems that contractility
660 better predicts contact guidance on aligned collagen fibrils that are stiff and cannot be remodeled
661 (collagen fibrils assembled on mica). Myosin phosphorylation is elevated in environments when cells can

662 recruit fibrils [46], but we assessed myosin phosphorylation on tissue culture plastic due to the infeasibility
663 of using western blotting to assess myosin phosphorylation on our aligned collagen fibril substrates
664 containing a small number of cells compared to that needed for western blotting. This likely explains the
665 ability of our measures of contractility to track less well with directionality index on collagen fibrils
666 assembled on mica. We measured myosin phosphorylation using immunofluorescence on collagen fibrils
667 assembled on mica, but the interpretation can be challenging due to the inability to properly quantify the
668 signal for dramatically different morphologies. For instance, rounded cells on soft substrates showed the
669 largest myosin phosphorylation level. Multiple studies underscore the role of contractility in cell
670 alignment and contact guidance [8,12,16,19,28,29]. While early migration stages are contractility-independent,
671 later stages require actomyosin traction forces for effective contact guidance [40]. Studies on microcontact-
672 printed collagen lines further show that MTLn3 cell directionality is diminished after blocking
673 contractility [8]. In a variety of cells, blocking contractility reduced alignment along microgrooves,
674 weakening contact guidance [28,29]. Similarly, in 3D collagen gels, inhibiting contractility with blebbistatin
675 or a myosin phosphorylation blocker lowered directionality to levels observed on non-aligned substrates
676 in MDA-MB-231 cells [12,52]. Taken together myosin contractility is vitally important in contact guidance,
677 where enhanced myosin contractility leads to high fidelity contact guidance.
678 In addition to myosin contractility, we established that formins and Arp2/3 modulate contact
679 guidance in a reciprocal manner. In mesenchymal cells, formin inhibition decreases directionality index
680 indicating a diminished contact guidance fidelity, whereas Arp2/3 inhibition increases directionality index
681 indicating an enhanced contact guidance fidelity. Similar behavior is seen in epithelial cell migration,
682 where formin inhibition diminishes the residence time in parallel migration as well as the fraction of cells
683 in parallel migration, but increases the fraction of cells in perpendicular migration. Arp 2/3 on the other
684 hand seems to enhance the fraction of cells that migrate parallel to the aligned collagen. Our motivation
685 for examining how both formins and Arp2/3 control directionality flows from two observations. First, the
686 F-actin networks that formins and Arp2/3 create are distinct in nature. Formins generate linear F-actin
687 structures like various forms of stress fibrils that help the cell form and maintain traction in a particular
688 direction of migration through stable focal adhesions attached to the ECM. Arp2/3 generates branched F-
689 actin networks that constitute the lamellipodium, a rounded structure that can also facilitate dynamic
690 adhesion and can bias migration in a particular direction but has much more plastic control of directional
691 persistence. Second, it has been elegantly shown in a variety of contexts that G-actin can be limiting, so
692 diminishing of linear F-actin structures through formin inhibition results in more branched F-actin
693 structures and vice versa, setting up feedback for reciprocal control by these two distinct F-actin networks
694 [41,53]. While the reciprocal regulation of contact guidance occurs at high formin (~20 μM) and Arp2/3
695 (~25 μM) inhibitor concentrations, submaximal concentrations produce results that are difficult to

696 reconcile. For instance, submaximal formin inhibitor concentrations show enhanced contact guidance and
697 submaximal Arp2/3 inhibitor concentrations show diminished contact guidance. Future work will be
698 geared toward understanding these results in the broad context of formin and Arp2/3 regulation. However,
699 very little work to date has examined the role of formins and Arp2/3 in contact guidance. In 1D contact
700 guidance systems, where cells are confined to 1D migration only, formins are important, whereas Arp2/3
701 is dispensable in maintaining speed [36,54,55]. However, these 1D systems dimensionally restrict migration
702 in a way that does not allow the assessment of how directional fidelity is controlled. In 2D systems of
703 contact guidance that include microcontact printed lines and ridges, formins seem to play a positive role
704 in controlling directional fidelity, agreeing with our results [34,37]. On the other hand the role of Arp2/3 is
705 less clear. Work exploring contact guidance on flexible substrates indicates that inhibiting Arp2/3
706 diminishes contact guidance [34] whereas other work on stiff substrates indicates that inhibiting Arp2/3
707 enhances contact guidance [37]. The current work adds evidence to the positive role of formins and the
708 negative role of Arp2/3 in enhancing contact guidance.
709 Finally, we have discovered a new mode of migration on aligned collagen fibrils for epithelial
710 cell migration. On strong contact guidance cues like ridges and lines of ECM, most all cells respond by
711 migrating parallel to the groove or line direction. As mentioned above our collagen fibril substrates reveal
712 cell type differences that can be masked in these other systems and these differences map to responses
713 observed in 3D. This was demonstrated by the difference between migration of mesenchymal cells, which
714 migrate on collagen fibrils with high fidelity and amoeboid cells, which essentially ignore the collagen
715 fibril direction. We find that epithelial cells can migrate in both a parallel and perpendicular fashion. This
716 behavior is only revealed when examining cell migration and is less apparent when examining cell
717 alignment in fixed images. This appears to be a new phenotype not observed by those examining fixed
718 cell morphology and one that is more readily observable using our aligned collagen fibril system.
719 Normally, during wound healing, collective migration occurs resulting in re-epithelialization of the
720 wound. However, we imagine that in some instances single cells detach or are left during injury. As the
721 wound develops, they interact with aligned fibrin or collagen fiber networks that are generated by
722 contractile dermal fibroblasts. It might be crucial for these cells to be somewhat agnostic to the directional
723 alignment of the collagen, necessitating both parallel and perpendicular migration. Alternatively, this
724 single-cell multi-directional phenotype might indicate similar collective cell responses on aligned
725 collagen fibrils that has not yet been observed. Indeed, work has been carried out trying to understand
726 collective cell migration on contact guidance cues and sheets indeed prefer migration parallel to the
727 groove, but again, perhaps there are some responses that are masked by these non-fibril systems [56–58].
728 External signals, such as stiffness, regulate the balance of perpendicular and parallel migration and both
729 formins and Arp2/3 play similar roles in epithelial cells as they do in mesenchymal cells in facilitating

730 and inhibiting contact guidance. This may be a single-cell specific phenotype, given that inhibiting
731 Arp2/3 in collective migration seems to diminish directional persistence in collective sheet migration on
732 grooves [56]. However, collective migration is intimately tied to cell-cell contacts, which depend on
733 Arp2/3 and, when disrupted, may negatively impact directional fidelity. How the F-actin structure
734 dynamically changes during parallel and perpendicular migration as well as how formins and Arp2/3
735 regulate this behavior differently during each mode of migration is still an open question and will need to
736 be assessed in the future. The discovery of this additional mode of directional migration likely reveals
737 important features of the ECM that regulate wound healing and could be encoded into tissue engineered
738 constructs to facilitate directed migration.

5. Conclusions:

We show that dermal fibroblasts are strong and can delaminate collagen fibrils from the surface of mica unless these fibrils are transferred and covalently attached to other substrates. Mesenchymal cells engage in robust contact guidance, whereas epithelial cells and amoeboid cells contact guide with lower fidelity. Contact guidance is strongly correlated with the contractile ability of cells. Cancer cells are more sensitive to stiffness during contact guidance than non-transformed cells, decreasing their directional fidelity on stiffer substrates. Formins and Arp2/3 reciprocally control contact guidance, where formins facilitate better contact guidance and Arp2/3 facilitates poorer contact guidance. Finally, epithelial cells appear to switch between parallel and perpendicular migration on aligned fibrils. This behavior is stiffness-dependent, where stiffer environments result in better contact guidance at slower rates. Formins enhance the parallel movement, whereas Arp2/3 has a richer control over contact guidance, diminishing parallel migration, but also decreasing perpendicular fraction.

Acknowledgements:

We acknowledge Curtis Mosher and the Roy J. Carver High Resolution Microscopy Facility.
This work was supported by the National Institutes of Health under grant No. GM143302.

Data Availability Statement

The data that support the findings of this study are available from the corresponding author upon reasonable request.

Conflict of Interest

The authors declare that there are no conflicts of interest regarding the publication of this manuscript.

References:

[1] N. R. Chevalier, Y. Ammouche, A. Gomis, L. Langlois, T. Guilbert, P. Bourdoncle, S. Dufour, *Commun Biol* **2021**, *4*, 770.

[2] W. D. Martinson, R. McLennan, J. M. Teddy, M. C. McKinney, L. A. Davidson, R. E. Baker, H. M. Byrne, P. M. Kulesa, P. K. Maini, *eLife* **2023**, *12*, e83792.

[3] O. A. Peña, P. Martin, *Nat Rev Mol Cell Biol* **2024**, *25*, 599.

[4] M. Ottosson, A. Jakobsson, F. Johansson, *PLoS One* **2017**, *12*, e0169419.

[5] A. Ray, P. P. Provenzano, *Curr Opin Cell Biol* **2021**, *72*, 63.

[6] C. R. Drifka, A. G. Loeffler, K. Mathewson, A. Keikhosravi, J. C. Eickhoff, Y. Liu, S. M. Weber, W. J. Kao, K. W. Eliceiri, *Oncotarget* **2016**, *7*, 76197.

[7] F. Yang, R. Murugan, S. Wang, S. Ramakrishna, *Biomaterials* **2005**, *26*, 2603.

[8] N. R. Romsey, Y. Hou, L. Lara Rodriguez, I. C. Schneider, *Cel. Mol. Bioeng.* **2014**, *7*, 122.

[9] A. D. Doyle, F. W. Wang, K. Matsumoto, K. M. Yamada, *Journal of Cell Biology* **2009**, *184*, 481.

[10] A. I. Teixeira, G. A. Abrams, P. J. Bertics, C. J. Murphy, P. F. Nealey, *Journal of Cell Science* **2003**, *116*, 1881.

[11] G. Thrivikraman, A. Jagiełło, V. K. Lai, S. L. Johnson, M. Keating, A. Nelson, B. Schultz, C. M. Wang, A. J. Levine, E. L. Botvinick, R. T. Tranquillo, *Proceedings of the National Academy of Sciences* **2021**, *118*, e2024942118.

[12] J. A. M. Nuhn, A. M. Perez, I. C. Schneider, *Acta Biomater* **2018**, *66*, 248.

[13] A. Ahmed, M. Mansouri, I. M. Joshi, A. M. Byerley, S. W. Day, T. R. Gaborski, V. V. Abhyankar, *Biofabrication* **2022**, *14*, 035019.

[14] I. M. Joshi, M. Mansouri, A. Ahmed, D. De Silva, R. A. Simon, P. Esmaili, D. E. Desa, T. M. Elias, E. B. Brown III, V. V. Abhyankar, *Advanced Functional Materials* **2024**, *34*, 2308071.

[15] A. Ray, Z. M. Slama, R. K. Morford, S. A. Madden, P. P. Provenzano, *Biophys J* **2017**, *112*, 1023.

[16] D. Caballero, L. Palacios, P. P. Freitas, J. Samitier, *Advanced Functional Materials* **2017**, *27*, 1702322.

[17] A. Ray, R. K. Morford, P. P. Provenzano, *Current Protocols in Stem Cell Biology* **2018**, *46*, e57.

[18] J. Wang, J. W. Petefish, A. C. Hillier, I. C. Schneider, *Langmuir* **2015**, *31*, 307.

[19] J. Wang, I. C. Schneider, *Biomaterials* **2017**, *120*, 81.

[20] J. Wang, J. Koelbl, A. Boddupalli, Z. Yao, K. M. Bratlie, I. C. Schneider, *Integr Biol (Camb)* **2018**, *10*, 705.

[21] D. C. Stewart, B. K. Brisson, W. K. Yen, Y. Liu, C. Wang, G. Ruthel, D. Gullberg, R. L. Mauck, M. Maden, L. Han, S. W. Volk, *J Invest Dermatol* **2024**, *0*.

[22] A. E. Woessner, J. D. McGee, J. D. Jones, K. P. Quinn, *Wound Repair and Regeneration* **2019**, *27*, 711.

[23] E.-M. Kamionka, B. Qian, W. Gross, F. Bergmann, T. Hackert, C. A. Beretta, N. Dross, E. Ryschich, *Cancers* **2021**, *13*, 3648.

[24] H. C. Pruitt, D. Lewis, M. Ciccaglione, S. Connor, Q. Smith, J. W. Hickey, J. P. Schneck, S. Gerecht, *Matrix Biology* **2020**, *85–86*, 147.

[25] P. P. Provenzano, K. W. Eliceiri, J. M. Campbell, D. R. Inman, J. G. White, P. J. Keely, *BMC Medicine* **2006**, *4*, 38.

[26] S. A. Fraser, Y.-H. Ting, K. S. Mallon, A. E. Wendt, C. J. Murphy, P. F. Nealey, *J Biomed Mater Res A* **2008**, *86*, 725.

[27] A. Sales, K. Ende, J. Diemer, A. R. Kyvik, J. Veciana, I. Ratera, R. Kemkemer, J. P. Spatz, J. Guasch, *ACS Omega* **2019**, *4*, 1791.

[28] A. Ray, O. Lee, Z. Win, R. M. Edwards, P. W. Alford, D.-H. Kim, P. P. Provenzano, *Nat Commun* **2017**, *8*, 14923.

[29] J. Comelles, V. Fernández-Majada, V. Acevedo, B. Rebollo-Calderon, E. Martínez, *Mater Today Bio* **2023**, *19*, 100593.
[30] M. Pourjafar, V. K. Tiwari, *Front. Cell Dev. Biol.* **2024**, *12*.
[31] E. Sahai, C. J. Marshall, *Nat Cell Biol* **2003**, *5*, 711.
[32] L. Isert, M. Passi, B. Freystetter, M. Grab, A. Roidl, C. Müller, A. Mehta, H. G. Sundararaghavan, S. Zahler, O. M. Merkel, *Materials Today Bio* **2025**, *30*, 101401.
[33] B. Yi, Y. Shen, H. Tang, X. Wang, Y. Zhang, *Acta Biomater* **2020**, *108*, 237.
[34] E. D. Tabdanov, V. Puram, A. Zhovmer, P. P. Provenzano, *Cell Reports* **2018**, *25*, 328.
[35] Q. Sun, X. Pan, P. Wang, Q. Wei, *Nano Lett.* **2024**, *24*, 6376.
[36] P. Monzo, Y. K. Chong, C. Guetta-Terrier, A. Krishnasamy, S. R. Sathe, E. K. F. Yim, W. H. Ng, B. T. Ang, C. Tang, B. Ladoux, N. C. Gauthier, M. P. Sheetz, *Molecular Biology of the Cell* **2016**, *27*.
[37] G. R. Ramirez-San Juan, P. W. Oakes, M. L. Gardel, *MBoC* **2017**, *28*, 1043.
[38] J. R. Tse, A. J. Engler, *Current Protocols in Cell Biology* **2010**, *47*, 10.16.1.
[39] K. E. Kubow, V. D. Shuklis, D. J. Sales, A. R. Horwitz, *Sci Rep* **2017**, *7*, 14380.
[40] A. Sales, A. W. Holle, R. Kemkemer, *Soft Matter* **2017**, *13*, 5158.
[41] C. Suarez, D. R. Kovar, *Nat Rev Mol Cell Biol* **2016**, *17*, 799.
[42] Y. Nishimura, S. Shi, F. Zhang, R. Liu, Y. Takagi, A. D. Bershadsky, V. Viasnoff, J. R. Sellers, *Journal of Cell Science* **2021**, *134*, jcs253708.
[43] J. Wang, I. C. Schneider, *Biomaterials* **2017**, *120*, 81.
[44] S. Ribeiro, A. Watigny, Y. Bayon, M. Biggs, D. I. Zeugolis, *Advanced NanoBiomed Research* **2024**, *4*, 2300042.
[45] I. A. Janson, A. J. Putnam, *J Biomed Mater Res A* **2015**, *103*, 1246.
[46] X. Dong, Q. Sun, J. Geng, X. Liu, Q. Wei, *Nano Lett.* **2024**, *24*, 4029.
[47] W. Y. Wang, C. D. Davidson, D. Lin, B. M. Baker, *Nat Commun* **2019**, *10*, 1186.
[48] Y. Xin, K. Li, M. Huang, C. Liang, D. Siemann, L. Wu, Y. Tan, X. Tang, *Oncogene* **2023**, *42*, 3457.
[49] J. A. Dombroski, J. M. Hope, N. S. Sarna, M. R. King, *Cells* **2021**, *10*, 2815.
[50] H. B. Aydin, A. Ozcelikkale, A. Acar, *ACS Biomater. Sci. Eng.* **2024**, *10*, 4682.
[51] M. R. Zanotelli, J. Zhang, C. A. Reinhart-King, *Cell Metabolism* **2021**, *33*, 1307.
[52] P. P. Provenzano, D. R. Inman, K. W. Eliceiri, S. M. Trier, P. J. Keely, *Biophysical Journal* **2008**, *95*, 5374.
[53] X. L. Chua, C. S. Tong, M. Su, X. J. Xǔ, S. Xiao, X. Wu, M. Wu, *Cell Reports* **2024**, *43*.
[54] K. Sheets, S. Wunsch, C. Ng, A. S. Nain, *Acta Biomaterialia* **2013**, *9*, 7169.
[55] C. Guetta-Terrier, P. Monzo, J. Zhu, H. Long, L. Venkatraman, Y. Zhou, P. Wang, S. Y. Chew, A. Mogilner, B. Ladoux, N. C. Gauthier, *Journal of Cell Biology* **2015**, *211*, 683.
[56] M. Lacroix, B. Smeets, C. Blanch-Mercader, S. Bell, C. Giuglaris, H.-Y. Chen, J. Prost, P. Silberzan, *Nat. Phys.* **2024**, *20*, 1324.
[57] Z. Chen, Q. Li, S. Xu, J. Ouyang, H. Wei, *Journal of Biomedical Nanotechnology* **2021**, *17*, 1079.
[58] C. Londono, M. J. Loureiro, B. Slater, P. B. Lücker, J. Soleas, S. Sathananthan, J. S. Aitchison, A. J. Kabla, A. P. McGuigan, *Proceedings of the National Academy of Sciences* **2014**, *111*, 1807.

Author Contributions:

A.F.: Conceived experiments, conducted experiments, analyzed the data and interpreted the data across all figures, prepared the figures, wrote the article and edited the article. S.T.: Wrote code and analyzed the data in **Figures 1-8** and **Supplementary Figures 2-8**. S.A.S.: Conceived experiments, conducted experiments, analyzed the data and interpreted the data in **Figures 3-5** and **Supplementary Figures 3-5**, wrote article and edited the article. F.R.N.: Conceived experiments, conducted experiments, analyzed data and interpreted the data in **Figure 3** and **Supplementary Figure 3**, wrote article and edited the article. I.C.S.: Conceived experiments, analyzed the data and interpreted the data across all figures, wrote the article, prepared the figures and edited the article.

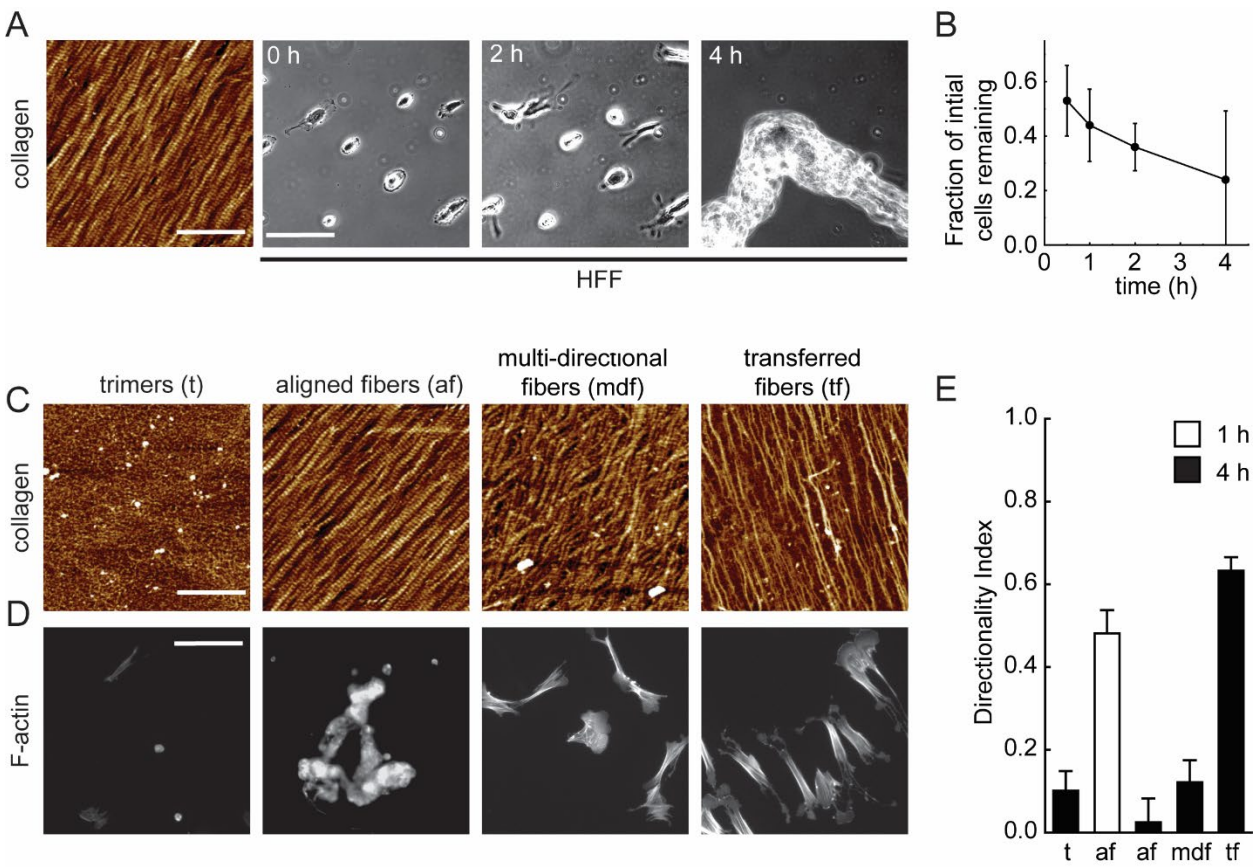

Figure 1: Contractile fibroblasts respond differently on different collagen substrates. (**A**) AFM image of collagen assembled on mica. AFM scale bar is 1 µm. Live-cell phase contrast microscopy images of HFFs on mica at 0, 2, and 4 h. Phase contrast image scale bar is 150 µm. (**B**) Fraction of initial cells remaining on the mica surface over time as assessed after fixation. $N_{samples} \geq 4$, $N_{cells} \geq 265$ and $N_{images} \geq 15$ (**C**) Various collagen patterns assembled on mica under different conditions. Trimers (t): citric acid buffer (pH 4.3) with 200 mM KCl, 10 µg/ml collagen and a 12 hours incubation. Aligned fibrils (af): 50 mM Tris buffer (pH 9.2) with 200 mM KCl, 10 µg/ml collagen and a 12 hours incubation. Multi-directional fibrils (mdf): 50 mM Tris buffer (pH 9.2) with 200 mM KCl, 100 µg/ml collagen and a 12 hours incubation. Transferred fibrils (tf): 50 mM Tris buffer (pH 9.2) with 200 mM KCl, 10 µg/ml collagen, a 12 hour incubation and transferred onto functionalized glass. Scale bar is 1 µm. (**D**) Phalloidin staining showing F-actin structure and HFF morphology on collagen fibrils under the same conditions as in C. Scale bar is 150 µm. (**E**) Directionality index of HFFs on different collagen patterns and after different incubation times on the collagen fibrils. $N_{samples} \geq 2$ and $N_{cells} \geq 122$. Error bars are 95% confidence intervals.

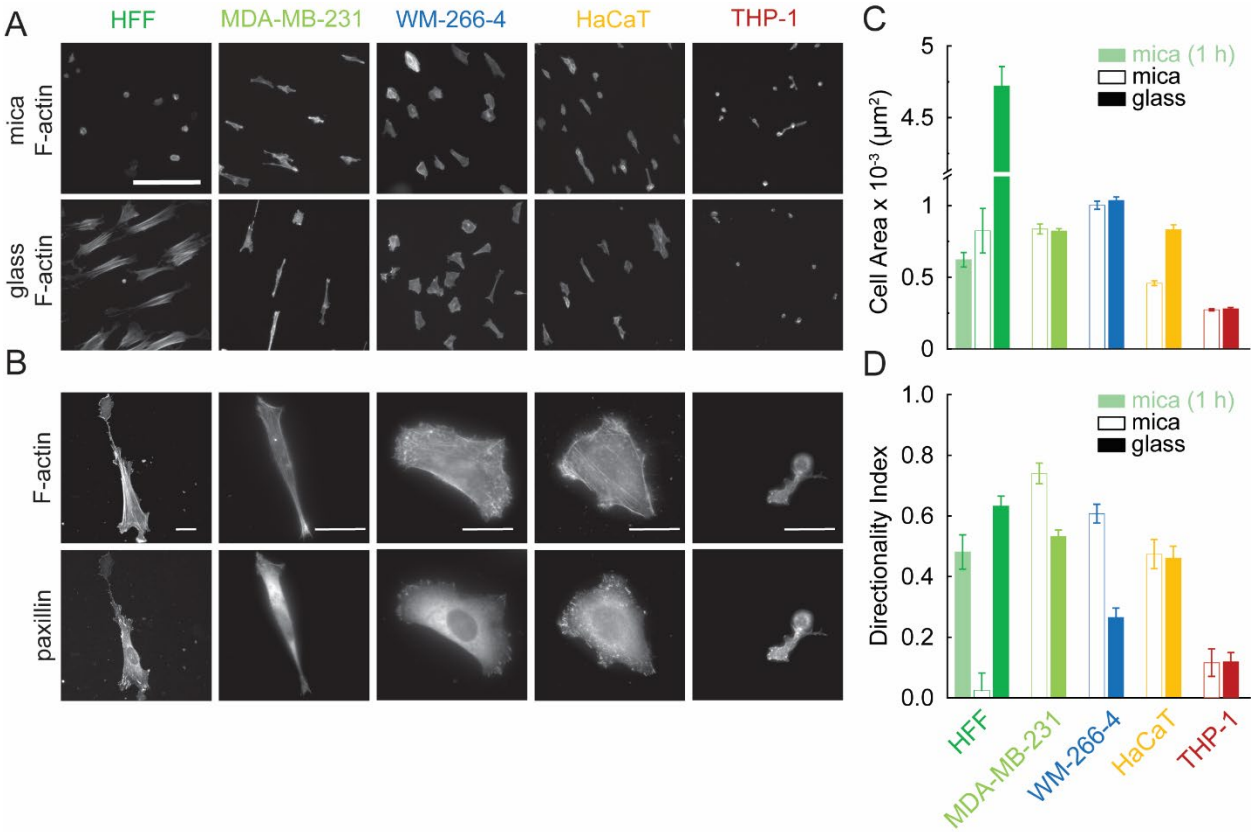

Figure 2: Different cells spread and align to different extents on aligned collagen fibrils. (**A**) F-actin staining of cells on both mica (top) and glass (bottom). Scale bar is 200 μm. (**B**) High resolution of F-actin and paxillin staining of cells on glass. Scale bars are 25 μm. Cell (**C**) area ($N_{samples} \geq 2$ and $N_{cells} \geq 152$) and (**D**) Directionality index ($N_{samples} \geq 2$ and $N_{cells} \geq 122$) of different cell lines plated on collagen fibrils on mica (open bars) or those transferred to glass (solid bars). Error bars represent 95% confidence intervals.

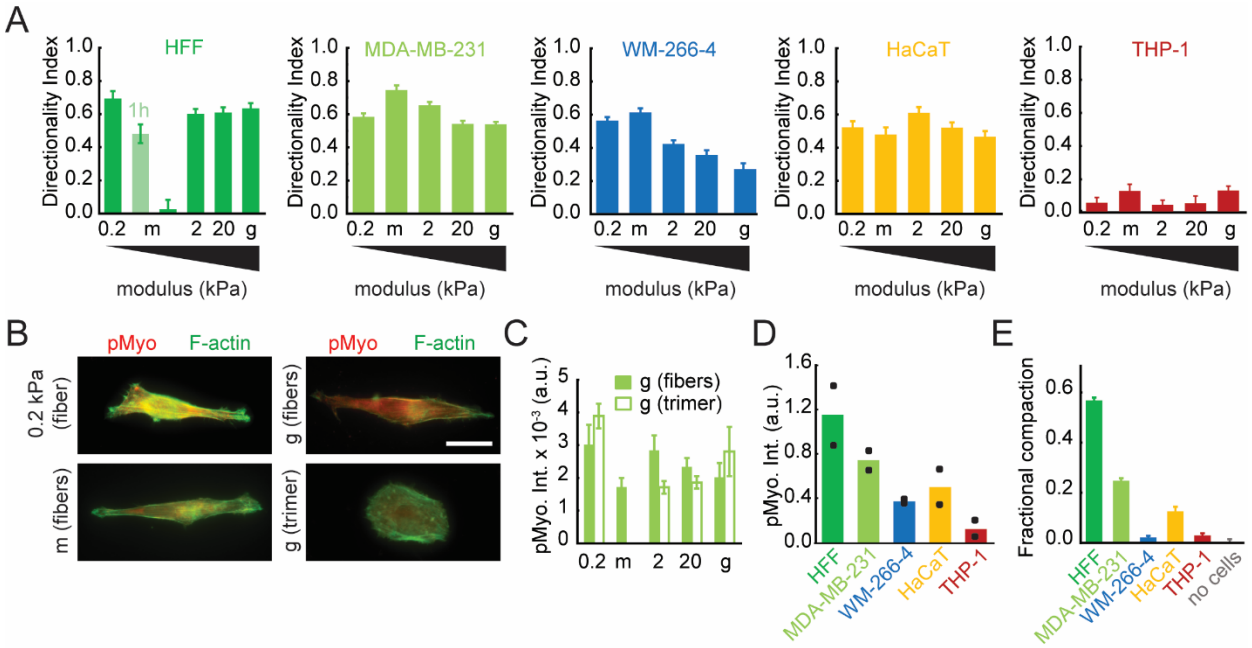

Figure 3: Higher contractile cells engage in optimal contact guidance at lower stiffness. (**A**) Directionality index of various cell lines on different substrates, including 0.2 kPa PAA (0.2), mica (m), 2 kPa PAA (2), 20 kPa PAA (20) and glass (g). $N_{samples} = 2$ and $N_{cells} = 122$. (**B**) F-actin (green) and phosphomyosin (pMyo, red) localization in MDA-MB-231 cells on 0.2 kPa PAA gel with transferred fibrils, glass (g) with transferred fibrils, mica (m) with aligned fibrils, and glass (g) with deposited collagen trimers. The scale bar is 25 µm. (**C**) Phosphorylated myosin (pMyo) intensity in immunofluorescence images of fixed MDA-MB-231 cells on various substrates, including 0.2 kPa PAA gel (0.2), mica (m), 2 kPa PAA (2), 20 kPa PAA (20), and glass (g) with both collagen fibrils (solid bars) and trimers (open bars), $N_{samples} \geq 2$ and $N_{cells} \geq 28$. (**D**) Phosphorylated myosin (pMyo) intensity from western blots. $N_{samples} \geq 2$. (**E**) Fractional compaction calculated from initial and 48 hours diameters of collagen gels across all cell lines. $N_{samples} \geq 3$. Error bars represent 95% confidence intervals.

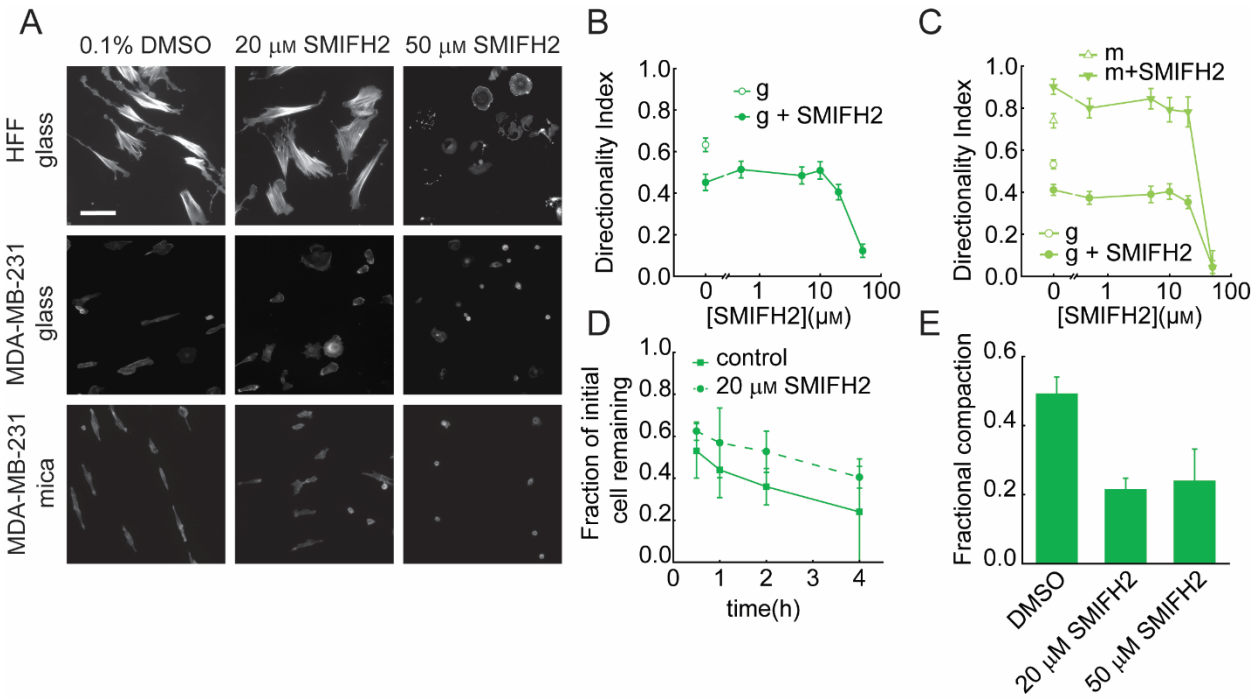

Figure 4: Formins inhibition marginally disrupts mesenchymal cell alignment and collagen fibril delamination, but dramatically diminishes gel compaction. (**A**) Immunofluorescence images of F-actin localization in HFF and MDA-MB-231 cells treated with 0.1% DMSO, 20 μM SMIFH2 and 50 μM SMIFH2 on both mica (m) and glass (g) substrates. The scale bar is 100 μm. (**B**) Directionality index of HFF cells treated with varying concentrations of SMIFH2 on glass (g) substrates, $N_{samples} \geq 3$ and $N_{cells} \geq 708$. The open circles at 0 μM SMIFH2 are cells without any treatment and the solid circles are cells treated with 0.1% DMSO. (**C**) Directionality index of MDA-MB-231 cells treated with different concentrations of SMIFH2 on both mica (m) and glass (g) substrates, $N_{samples} \geq 1$ and $N_{cells} \geq 53$. (**D**) Fraction of initial HFF cells treated with and without 20 μM SMIFH2 remaining on the mica surface over time as assessed after fixation, $N_{samples} \geq 4$, $N_{cells} \geq 265$ and $N_{images} \geq 15$ (**E**) Fractional compaction of HFF cells treated with different concentrations of SMIFH2 calculated from initial and 48 hour diameters of collagen gels, $N_{samples} \geq 3$. Error bars represent 95% confidence intervals.

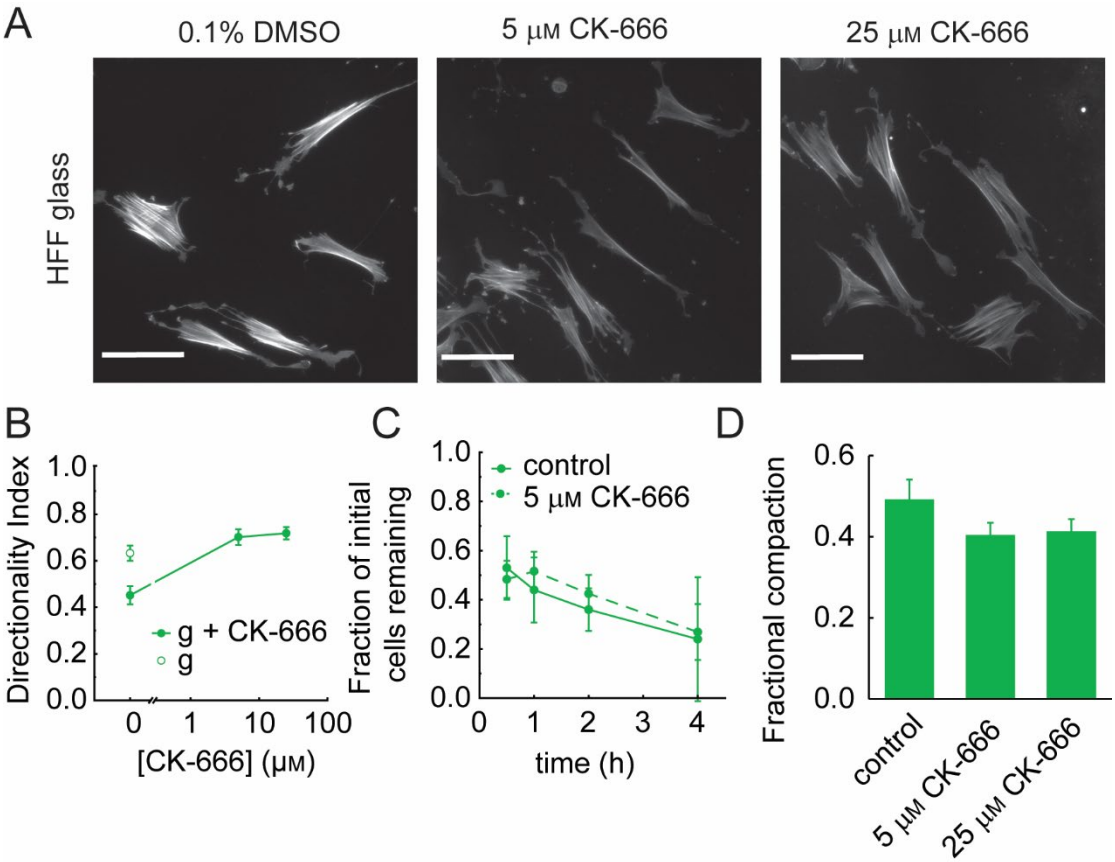

Figure 5: Arp2/3 inhibition enhances mesenchymal cell alignment, but does not robustly affect collagen fibril delamination or collagen gel compaction. (**A**) Immunofluorescence images of F-actin localization in HFF cells treated with 5 μM and 25 μM of CK-666 fixed on glass (g). The scale bar is 100 μm. (**B**) Directionality index of fixed HFF cells on glass substrates as a function of CK-666 concentration including 5 and 25 μM CK-666. The open circles at 0 μM SMIFH2 are cells without any treatment and the solid circles are cells treated with 0.1% DMSO, $N_{samples} \geq 3$ and $N_{cells} \geq 594$ (**C**) Fraction of initial HFF cells treated with or without 5 μM CK-666 remaining on the mica surface over time as assessed after fixation, $N_{samples} \geq 4$, $N_{cells} \geq 256$ and $N_{images} \geq 15$. (**D**) Fractional compaction of HFF cells treated with different concentrations of CK-666 calculated from initial and 48 h diameters of collagen gels across all cell lines, $N_{samples} \geq 3$. Error bars represent 95% confidence intervals.

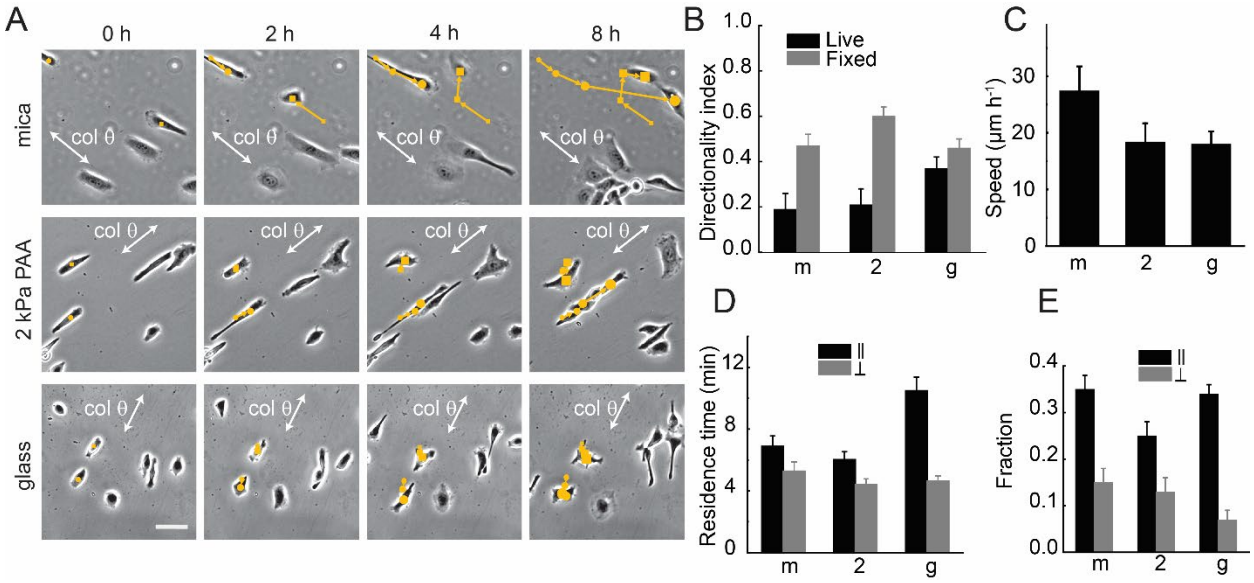

Figure 6: Epithelial cells exhibit both parallel and perpendicular movement that generates low directionality. (**A**) Phase contrast, live cell migration montages of HaCaT cells on different substrates: mica (m), 2 kPa PAA (2), and glass (g). Circles and squares mark previous cell positions. The collagen fibril direction is denoted with the white arrow (col θ). The scale bar is 50 μm. (**B**) Directionality index and (**C**) cell speed, fixed cells: $N_{samples} \geq 3$ and $N_{cells} \geq 483$, and live cells: $N_{samples} \geq 4$ and $N_{cells} \geq 41$. (**D**) Residence time, indicating the duration cells spend in parallel or perpendicular migration with respect to collagen fibrils and (**E**) fraction of migration steps taken by cells in parallel and perpendicular directions relative to collagen fibrils, $N_{samples} \geq 4$ and $N_{cells} \geq 41$. Error bars represent 95% confidence intervals.

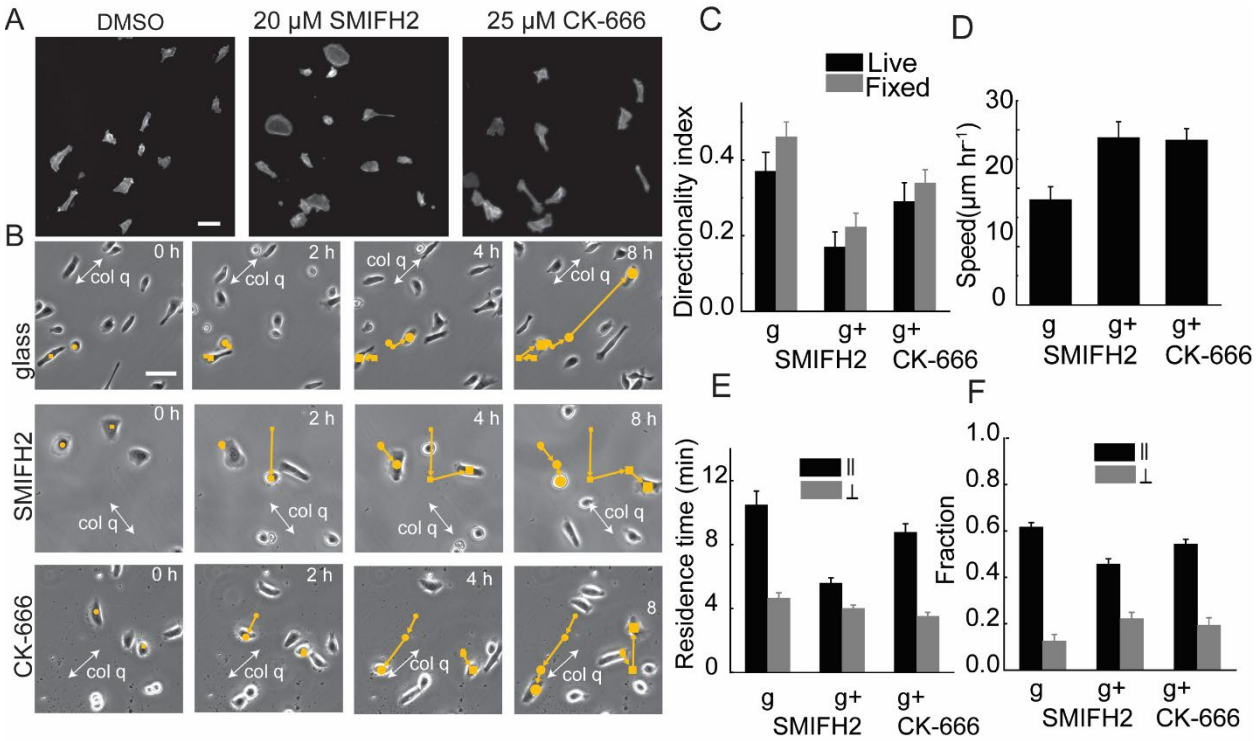

924

925 **Figure 7: In epithelial cells Arp2/3 inhibition increases parallel and perpendicular migration,**
926 **whereas formins inhibition increases perpendicular migration only. (A)** immunofluorescence images
927 of HaCaT cells fixed on glass treated with 0.1% DMSO, 20 μM SMIFH2 and 25 μM CK-666. Scale bar is
928 50μm (**B**) Live cell migration montages of HaCaT cells on glass without inhibitors, with 20 μM SMIFH2
929 and with 25 μM CK-666. Scale bar is 50 μm (**C**) Directionality index of both fixed $N_{samples} \geq 4$ and $N_{cells} \geq$
930 712 and live cells .$N_{samples} \geq 5$ and $N_{cells} \geq 85$ under different conditions: no inhibitor, 20 μM SMIFH2 and
931 25 μM CK-666. (**D**) Cell speed calculated from live cell migration under the same conditions: no
932 inhibitor, 20 μM SMIFH2 and 25 μM CK-666, $N_{samples} \geq 5$ and $N_{cells} \geq 85$ (**E**) Average residence time of
933 cells moving parallel (less than 30° deviation) or perpendicular (more than 60° deviation) to collagen
934 fibrils. $N_{samples} \geq 5$ and $N_{cells} \geq 85$ (**F**) Fraction of cells moving parallel (deviation less than 30°) or
935 perpendicular (deviation more than 60°) to collagen fibrils. $N_{samples} \geq 5$ and $N_{cells} \geq 85$.

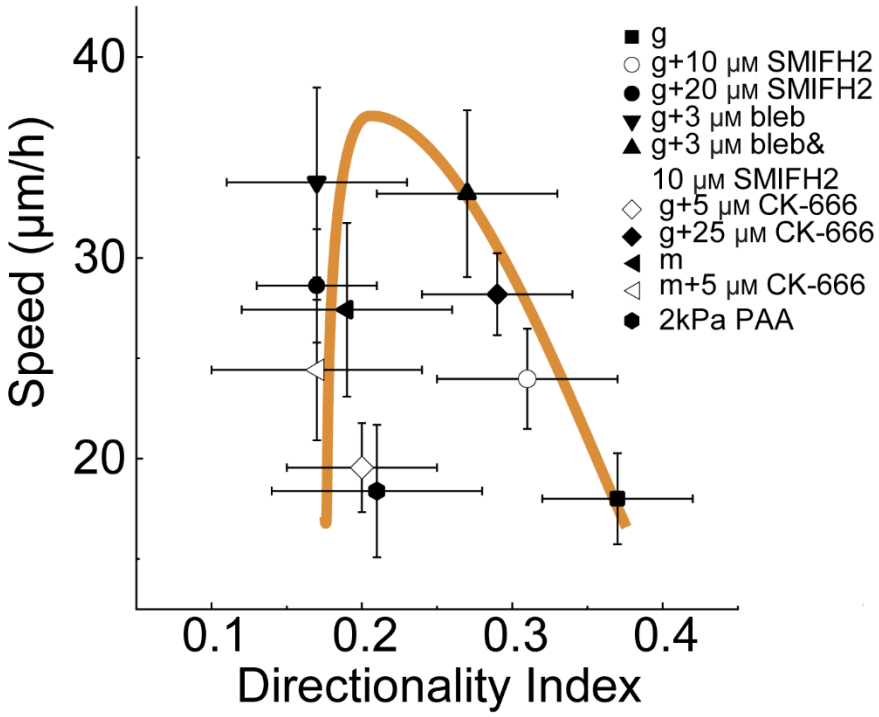

Figure 8: Epithelial cells demonstrate a biphasic dependence of speed on directionality in response to a variety of stiffness and F-actin regulatory protein inhibitors. The speed and directionality index calculated from live cell migration of HaCaT Cell on various conditions. $N_{samples} \geq 4$ and $N_{cells} \geq 41$ and error bars represent 95% confidence intervals.